CREEP IN SHELLS OF REVOLUTION

SUMIO MURAKAMI

Department of Mechanical Engineering

(Received September 21, 1971)

CONTENTS

General Introduction

Recent development in the field of technology which has space- and nuclear-engineering as its leading parts has required not only the exploitation of superior high-temperature alloys which endure the severe conditions of high temperature and high stress, but also has required the research of analytical methods of stress and strain in the various equipments or structures employed in such conditions. In these equipments, in general, creep deformation which proceeds with time even under the constant load and the constant temperature is significant. In order to secure the high performance and the high safety in the design of them, therefore, it is indispensable to take account of the creep deformation over the whole service life besides the elastic-plastic deformation which occurs at the instant of loading.

In many metals employed in engineering practice, when loaded with a constant stress at the presence of high temperature, the strain rate decreases rapidly at first, then tends to a constant asymptotically and finally increases again up to the rupture. These three stages are called those of transient creep, steady-state creep and accelerating creep, respectively. In the present paper, we investigate the transient and the steady-state creep deformation of shells of revolution which is one of the most important examples of the above mentioned high temperature equipments. The accelerating creep is, in general, omitted from the objective of creep design, because it is connected with very unstable stage just before the creep rupture.

The present problems have so far attracted considerable attention of many researchers because of their practical importance. Nevertheless, the rigorous treatment of them were quite lacking on account of the mathematical difficulty connected with the non-linear feature of creep. The previous papers were restricted either to those of approximate analyses due to some simplifications, or those connected with the thin spheres or the thin circular tubes without regard to the effect of end condition of shells which is the most important from the viewpoint of design.

The development of digital computers in these days, however, has enabled us to perform rigorous analyses of such problems numerically. In this paper, therefore, we develop a numerical approach to these problems by means of the finite-difference method or the extended Newton method combined with the method of finite-difference, and elucidate the features of creep deformation of shells of revolution employed under the condition of high temperature and high stress.

In Part I of the paper, the transient creep analyses of shells of revolution are discussed on the bases of the power creep law and the creep theories of the Mises-Mises, Tresca-Mises and Tresca-Tresca type. The strain-hardening and the time-hardening hypotheses are employed. As an example, the creep deformation and the associated state of stress are investigated for circular cylindrical shells of various shell-geometries and the various magnitudes of internal pressure. The difference between the creep theories as well as between the hardening hypotheses as applied to the present problem is also discussed. Calculations are performed for the constant and the variable internal pressure.

Part II, furthermore, is concerned with the analysis of the steady-state creep of shells according to the power creep law and the creep theory of the Mises-

Mises type. The extended Newton method combined with finite-difference procedure is applied. As numerical examples, creep in circular cylindrical shells as well as partial spherical shells is analysed. The effects of shell-geometry and creep exponent on the state of stress and deformation rate are investigated. The rigorous results for circular cylindrical shells obtained herein are also compared with the previous solutions for the sandwich shells, and the validity of the assumption of sandwich construction is discussed.

Notation

Dimensional quantities (Fig. 1.1)

x, y, z ; orthogonal co-ordinates in the directions tangential to the parallel of latitude and the meridian of shell of revolution, and that perpendicular to them.

r_0, r_1, r_2; radius of curvature of the parallel of latitude, and those of segments in the meridional plane and the plane perpendicular to it.

ϕ, θ ; angles specifying the parallel of latitude and the meridian.

β ; central semi-angle.

h ; thickness of shell.

X, Y, Z; components of external force in the x-, y- and z-directions.

v, w ; components of displacement in the y- and z-directions.

σ, ε ; stress and strain in the uniaxial state of stress.

σ_e, ε_e ; equivalent stress and equivalent strain.

$\sigma_\phi, \sigma_\theta, \varepsilon_\phi, \varepsilon_\theta$; components of stress and strain.

s_{ij}, e_{ij} ; components of deviatric stress and strain tensors.

$N_\phi, N_\theta, M_\phi, M_\theta$; components of membrane force and bending moment.

E, ν ; Young's modulus and Poisson's ratio.

A, n, m; material constants for transient creep.

k, n ; material constants for steady-state creep.

$\boldsymbol{A}, \boldsymbol{X}, \boldsymbol{B}$; coefficient matrix, unknown column vector and inhomogeneous column vector.

λ ; relaxation parameter.

δ ; a small value specifying the accuracy of iterative procedure.

t ; time.

g ; difference interval.

N, N' ; numbers of divisions over the central semi-angle and that over the half thickness of shell.

c ; suffix referring to creep.

i ; suffix refferring to i-th mesh point.

$(\dot{\ })$; derivative with respect to time.

$(\ )^*$; approximate value.

$(\bar{\ })$; small difference between the approximate and actual values.

Non-dimensional quantities

(i) Transient creep

Circular cylindrical shell

$$\xi = \frac{x}{\left(\frac{l}{2}\right)}, \quad \eta = \frac{z}{\left(\frac{h}{2}\right)}, \quad V = \frac{v}{\left(\frac{\hat{p}al}{Eh}\right)}, \quad W = \frac{w}{\left(\frac{\hat{p}a^2}{Eh}\right)}, \quad E_x = \frac{\varepsilon_x}{\left(\frac{\hat{p}a}{Eh}\right)}, \quad E_\theta = \frac{\varepsilon_\theta}{\left(\frac{\hat{p}a}{Eh}\right)}$$

$$E_e=\frac{\varepsilon_e}{\left(\frac{\hat{p}a}{Eh}\right)},\quad S_x=\frac{\sigma_x}{\left(\frac{\hat{p}a}{h}\right)},\quad S_\theta=\frac{\sigma_\theta}{\left(\frac{\hat{p}a}{h}\right)},\quad S_e=\frac{\sigma_e}{\left(\frac{\hat{p}a}{h}\right)},\quad n_x=\frac{N_x}{\hat{p}a},\quad n_\theta=\frac{N_\theta}{\hat{p}a}$$

$$m_x=\frac{M_x}{\hat{p}ah},\quad m_\theta=\frac{M_\theta}{\hat{p}ah},\quad P=\frac{p}{\hat{p}},\quad \alpha^2=\frac{\sqrt{3(1-\nu^2)}}{4}\frac{l^2}{ah}$$

where

x ; co-ordinate in the axial direction.

l ; length of the shell.

a ; average radius.

p ; internal pressure.

$\hat{p}$; arbitrary reference pressure to define dimensionless variables.

α ; a parameter specifying the geometry of circular cylindrical shells[21].

Spherical shell

$$\eta=\frac{2z}{h},\quad V=\frac{v}{a\left(\frac{\hat{p}a}{2Eh}\right)},\quad W=\frac{w}{a\left(\frac{\hat{p}a}{2Eh}\right)},\quad E_\phi=\frac{\varepsilon_\phi}{\left(\frac{\hat{p}a}{2Eh}\right)},\quad E_\theta=\frac{\varepsilon_\theta}{\left(\frac{\hat{p}a}{2Eh}\right)}$$

$$E_e=\frac{\varepsilon_e}{\left(\frac{\hat{p}a}{2Eh}\right)},\quad S_\phi=\frac{\sigma_\phi}{\left(\frac{\hat{p}a}{2h}\right)},\quad S_\theta=\frac{\sigma_\theta}{\left(\frac{\hat{p}a}{2h}\right)},\quad S_e=\frac{\sigma_e}{\left(\frac{\hat{p}a}{2h}\right)},\quad n_\theta=\frac{N_\phi}{\left(\frac{\hat{p}a}{2}\right)}$$

$$n_\theta=\frac{N_\theta}{\left(\frac{\hat{p}a}{2}\right)},\quad m_\phi=\frac{M_\phi}{\left(\frac{\hat{p}ah}{2}\right)},\quad m_\theta=\frac{M_\theta}{\left(\frac{\hat{p}ah}{2}\right)},\quad H=\frac{h}{a}$$

(ii) Steady-state creep

Circular cylindrical shell

$$\xi=\frac{2x}{l},\quad \eta=\frac{2z}{h},\quad V=\frac{v}{lk\left(\frac{pa}{h}\right)^n},\quad W=\frac{w}{ak\left(\frac{pa}{h}\right)^n},\quad E_x=\frac{\varepsilon_x}{k\left(\frac{pa}{h}\right)^n},\quad E_\theta=\frac{\varepsilon_\theta}{k\left(\frac{pa}{h}\right)^n}$$

$$E_e=\frac{\varepsilon_e}{k\left(\frac{pa}{h}\right)^n},\quad S_x=\frac{\sigma_x}{\left(\frac{pa}{h}\right)},\quad S_\theta=\frac{\sigma_\theta}{\left(\frac{pa}{h}\right)},\quad S_e=\frac{\sigma_e}{\left(\frac{pa}{h}\right)},\quad n_x=\frac{N_x}{pa},\quad n_\theta=\frac{N_\theta}{pa}$$

$$m_x=\frac{M_x}{pah},\quad m_\theta=\frac{M_\theta}{pah},\quad \alpha^2=\frac{\sqrt{3(1-\nu^2)}}{4}\frac{l^2}{ah}=\frac{3}{8}\frac{l^2}{ah}\left(\nu=\frac{1}{2}\right)$$

Spherical shell

$$\eta=\frac{2z}{h},\quad V=\frac{v}{\frac{ka}{2}\left(\frac{pa}{2h}\right)^n},\quad W=\frac{w}{\frac{ka}{2}\left(\frac{pa}{2h}\right)^n},\quad E_\phi=\frac{\varepsilon_\phi}{\frac{k}{2}\left(\frac{pa}{2h}\right)^n},\quad E_\theta=\frac{\varepsilon_\theta}{\frac{k}{2}\left(\frac{pa}{2h}\right)^n}$$

$$E_e=\frac{\varepsilon_e}{\frac{k}{2}\left(\frac{pa}{2h}\right)^n},\quad S_\phi=\frac{\sigma_\phi}{\left(\frac{pa}{2h}\right)},\quad S_\theta=\frac{\sigma_\theta}{\left(\frac{pa}{2h}\right)},\quad S_e=\frac{\sigma_e}{\left(\frac{pa}{2h}\right)},\quad n_\phi=\frac{N_\phi}{\left(\frac{pa}{2}\right)}$$

$$n_\theta=\frac{N_\theta}{\left(\frac{pa}{2}\right)},\quad m_\phi=\frac{M_\phi}{\left(\frac{pah}{2}\right)},\quad m_\theta=\frac{M_\theta}{\left(\frac{pah}{2}\right)},\quad H=\frac{h}{a}$$

Part I. Transient Creep of Shells of Revolution[1)~4)]

1. Introduction

In the creep design of apparatuses employed under the severe conditions of high temperature and high stress, as the design life is relatively short, the stage of primary creep occupys major part of the total life-time and hence can never be neglected. Vessels subjected to internal pressure are examples of such apparatuses, and the informations on their behaviour in short time range are often required. Nevertheless, published works on the deformations of pressure vessels in this range are relatively scarce*.

If the total strain is assumed to consist of the primary creep and the elastic strain, the constitutive equation is linear with respect to the stress- and strain-rate. In the geometrically linear problems, therefore, the fundamental differential equations are also linear as regards these rates. If they are replaced by the corresponding difference equations, they yield the simultaneous linear equations, which can be easily solved.

In the present Part, creep behaviour of shells of revolution under various loading conditions is analysed by this method by assuming the power creep law and the creep theories of Mises-Mises, Tresca-Mises and Tresca-Tresca type. The strain-hardening and the time-hardening hypothesis are employed. In the analysis, attention is paid to the accuracy of the analysis in particular.

The first purpose of the present Part is to provide a method of transient creep analysis of shells of revolution, and to elucidate the typical feature of the creep deformation of particular shells with emphasis on the effect of shell geometry. The second purpose, furthermore, is to provide a comparison for facilitating a discussion of the validity of the above mentioned hardening hypotheses as applied to the transient creep of shells. Since strain-hardening and time-hardening hypotheses are employed most frequently to the transient creep analyses of various structures and moreover since it is generally accepted that the former is physically supported while the latter has the advantage of mathematical feasibility, their difference or validity has been examined repeatedly[13)]. These examinations, however, were mainly performed under uniform state of stress by means of thin tubular specimens, and the validity of these hardening hypotheses cannot be inferred therefrom when they are applied to the practical engineering problems. Consequently, it is interesing to investigate quantitatively the difference between both hypotheses in the case of circular cylindrical shells which are far from in the state of uniform stress as an example of such problems.

To show the difference of numerical results obtained by different creep theories and to discussed the suitable theory in the creep design of pressurised shells are the other purposed of this Part. The most common type of effective stress (and also effective strain) and flow rule adopted in multiaxial creep analyses are those of Mises and Tresca type[14)~16)]. Among the four kinds of combinations of them, the creep theories of Mises-Mises, Tresca-Mises (Tresca's effective stress and Mises' flow rule) and Tresca-Tresca type are used in practice usually. The creep theory of Mises-Mises type, above all, is most popular and has been postu-

* During the preparation of References [1]-[4], R. K. Penny[10)~12)] published several papers on the transient creep of pressurised shells based on the time-hardening hypothesis and creep theory of Mises-Mises type according to the similar procedure as that of the present Part.

lated in the majority of previous works. According to A. M. Wahl's results[18], however, the Tresca-Mises theory furnished a satisfactory coincidence with the experimental results, while Mises-Mises theory predicted smaller values of creep strain and, therofore, was on the unsafe side from the viewpoint of creep design. The similar trends were also found in creep deformation under the state of biaxial tension[19][20]. In the present Part, therefore, the difference between the numerical results due to these three kinds of creep theories in regard to the present example is also discussed.

2. Governing Equations

2.1. Equations for transient creep of shells of revolution

2.1.1. Basic relations

According to the small-deflection theory of shell, the equations of equilibrium and the kinematic relations for axisymmetric deformation of thin shells of revolution (Fig. 1.1) are expressed as follows[21]~[23]:

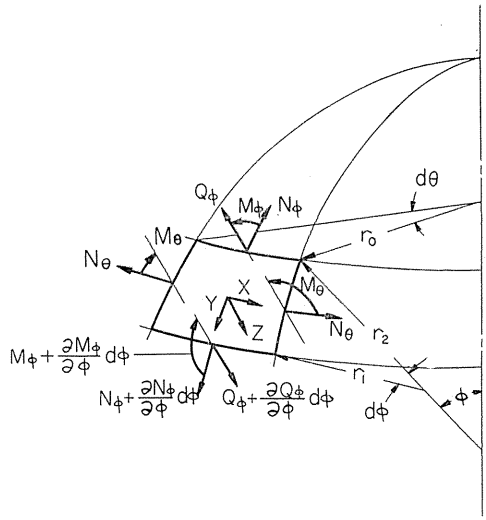

FIG. 1.1. Nomenclature.

$$\left.\begin{aligned}&\frac{d}{d\phi}(N_\phi r_0)-N_\theta r_1\cos\phi-\frac{1}{r_1}\frac{d}{d\phi}(M_\phi r_0)+M_\theta\cos\phi-Yr_0r_1=0\\&N_\phi r_0+N_\theta r_1\sin\phi+\frac{d}{d\phi}\left\{\frac{1}{r_1}\frac{d}{d\phi}(M_\phi r_0)-M_\theta\cos\phi\right\}-Zr_0r_1=0\end{aligned}\right\}\tag{1.1}$$

$$\left.\begin{aligned}&\varepsilon_\phi=\frac{1}{r_1}\frac{dv}{d\phi}-\frac{w}{r_1}-\frac{z}{r_1}\frac{d}{d\phi}\left(\frac{v}{r_1}+\frac{1}{r_1}\frac{dw}{d\phi}\right)\\&\varepsilon_\theta=\frac{v}{r_2}\cot\phi-\frac{w}{r_2}-\frac{z}{r_2}\cot\phi\left(\frac{v}{r_1}+\frac{1}{r_1}\frac{dw}{d\phi}\right)\end{aligned}\right\}\tag{1.2}$$

The non-vanishing components of the stress in the thin shells of revolution discussed here are σ_ϕ and σ_θ. Then, if the total strain-rate is assumed to be expressed by the sum of the elastic and the creep rate, the principal components

of strain rates are expressed by the relations

$$\dot{\varepsilon}_\phi = \frac{1}{E}(\dot{\sigma}_\phi - \nu\dot{\sigma}_\theta) + \dot{\varepsilon}_{\phi c}, \quad \dot{\varepsilon}_\theta = \frac{1}{E}(\dot{\sigma}_\theta - \nu\dot{\sigma}_\phi) + \dot{\varepsilon}_{\theta c} \tag{1.3}$$

By solving the above relations with respect to $\dot{\sigma}_\phi$, $\dot{\sigma}_\theta$ and expressing $\dot{\varepsilon}_\phi$, $\dot{\varepsilon}_\theta$ in terms of $\dot{v}$, $\dot{w}$ by means of (1.2), we obtain the following relations

$$\begin{bmatrix} \dot{\sigma}_\phi \\ \dot{\sigma}_\theta \end{bmatrix} = \frac{-E}{1-\nu^2}\left\{\begin{bmatrix} I_{11}\, I_{12} \cdots I_{15} \\ I_{21}\, I_{22} \cdots I_{25} \end{bmatrix}\begin{Bmatrix} \dot{v} \\ d\dot{v}/d\phi \\ \dot{w} \\ d\dot{w}/d\phi \\ d^2\dot{w}/d\phi^2 \end{Bmatrix} + \begin{bmatrix} \dot{G}_1 \\ \dot{G}_2 \end{bmatrix}\right\} \tag{1.4}$$

where

$$\left.\begin{aligned} I_{11} &= \frac{z}{r_1}\frac{d}{d\phi}\left(\frac{1}{r_1}\right) + \nu\frac{\cot\phi}{r_2}\left(\frac{z}{r_1} - 1\right), \quad I_{12} = \frac{1}{r_1}\left(\frac{z}{r_1} - 1\right) \\ I_{13} &= \left(\frac{1}{r_1} + \frac{\nu}{r_2}\right), \quad I_{14} = \frac{z}{r_1}\left[\frac{d}{d\phi}\left(\frac{1}{r_1}\right) + \nu\frac{\cot\phi}{r_2}\right], \quad I_{15} = \frac{1}{r_1}\frac{z}{r_1} \end{aligned}\right\} \tag{1.5 a}$$

$$\left.\begin{aligned} I_{21} &= \nu\frac{z}{r_1}\frac{d}{d\phi}\left(\frac{1}{r_1}\right) + \frac{\cot\phi}{r_2}\left(\frac{z}{r_1} - 1\right), \quad I_{22} = \frac{\nu}{r_1}\left(\frac{z}{r_1} - 1\right) \\ I_{23} &= \left(\frac{\nu}{r_1} + \frac{1}{r_2}\right), \quad I_{24} = \frac{z}{r_1}\left[\nu\frac{d}{d\phi}\left(\frac{1}{r_1}\right) + \frac{\cot\phi}{r_2}\right], \quad I_{25} = \frac{\nu}{r_1}\frac{z}{r_1} \end{aligned}\right\} \tag{1.5 b}$$

$$\dot{G}_1 = \dot{\varepsilon}_{\phi c} + \nu\dot{\varepsilon}_{\theta c}, \quad \dot{G}_2 = \dot{\varepsilon}_{\theta c} + \nu\dot{\varepsilon}_{\phi c} \tag{1.5 c}$$

Integration of (1.4) yields the following expressions for the rates of membrane force and bending moment:

$$\begin{Bmatrix} \dot{N}_\phi \\ \dot{N}_\theta \\ \dot{M}_\phi \\ \dot{M}_\theta \end{Bmatrix} = \begin{bmatrix} K_{11}\, K_{12} \cdots K_{15} \\ K_{21}\, K_{22} \cdots K_{25} \\ L_{11}\, L_{12} \cdots L_{15} \\ L_{21}\, L_{22} \cdots L_{25} \end{bmatrix}\begin{Bmatrix} \dot{v} \\ d\dot{v}/d\phi \\ \dot{w} \\ d\dot{w}/d\phi \\ d^2\dot{w}/d\phi^2 \end{Bmatrix} + \begin{Bmatrix} \dot{P}_1 \\ \dot{P}_2 \\ \dot{Q}_1 \\ \dot{Q}_2 \end{Bmatrix} \tag{1.6}$$

where

$$\left.\begin{aligned} K_{rs} &= \frac{-E}{1-\nu^2}\int_{-h/2}^{h/2} I_{rs}dz, \quad L_{rs} = \frac{-E}{1-\nu^2}\int_{-h/2}^{h/2} I_{rs}z dz \\ \dot{P}_r &= \frac{-E}{1-\nu^2}\int_{-h/2}^{h/2} \dot{G}_r dz, \quad \dot{Q}_r = \frac{-E}{1-\nu^2}\int_{-h/2}^{h/2} \dot{G}_r z dz, \quad (r = 1, 2\,;\ s = 1, 2, \ldots, 5) \end{aligned}\right\} \tag{1.7}$$

Now, let's assume that the relation between the creep strain ε_c at time t in the stage of transient creep and the relevant stress in the state of uniaxial stress is expressed as follows:

$$\varepsilon_c = A\sigma^n t^m \tag{1.8}$$

The above relation is valid for the majority of metals at elevated temperature under relatively low level of stress[14)~17)]. Differetiating (1.8) with respect to time, we obtain the strain rate according to the strain-hardening and the time-hardening hypothesis[14)~16)]:

$$\dot{\varepsilon}_c = mA^{1/m}\sigma^{n/m}\varepsilon_c^{(m-1)/m} \quad \text{(strain-hardening)} \tag{1.9a}$$

$$\dot{\varepsilon}_c = mA\sigma^n t^{m-1} \quad \text{(time-hardening)} \tag{1.9b}$$

By assuming the isotropy and the incompressibility of the material the above relations can be extended to the multiaxial state of stress. According to the three kinds of creep theories described previously, the components of creep rate in the present shells can be expressed as follows[14)15)]:

● Mises-Mises and Tresca-Mises theories

$$\left.\begin{aligned}\dot{\varepsilon}_{\phi c} &= mA^{1/m}\sigma_e^{(n-m)/m}\varepsilon_{ec}^{(m-1)/m}\left(\sigma_\phi - \frac{1}{2}\sigma_\theta\right)\\ \dot{\varepsilon}_{\theta c} &= mA^{1/m}\sigma_e^{(n-m)/m}\varepsilon_{ec}^{(m-1)/m}\left(\sigma_\theta - \frac{1}{2}\sigma_\phi\right)\end{aligned}\right\} \quad \text{(strain-hardening)} \tag{1.10a}$$

$$\left.\begin{aligned}\dot{\varepsilon}_{\phi c} &= mA\sigma_e^{n-1}t^{m-1}\left(\sigma_\phi - \frac{1}{2}\sigma_\theta\right)\\ \dot{\varepsilon}_{\theta c} &= mA\sigma_e^{n-1}t^{m-1}\left(\sigma_\theta - \frac{1}{2}\sigma_\phi\right)\end{aligned}\right\} \quad \text{(time-hardening)} \tag{1.10b}$$

where the effective stress and effective creep-strain are given by the following relations:

$$\left.\begin{aligned}\sigma_e &= (\sigma_\phi^2 - \sigma_\phi\sigma_\theta + \sigma_\theta^2)^{1/2}\\ \varepsilon_{ec} &= \frac{2}{\sqrt{3}}(\varepsilon_{\phi c}^2 + \varepsilon_{\phi c}\varepsilon_{\theta c} + \varepsilon_{\theta c}^2)^{1/2}\end{aligned}\right\} \quad \text{(Mises-Mises)} \tag{1.11}$$

$$\left.\begin{aligned}\sigma_e &= \mathrm{Max}\{|\sigma_\phi|,\ |\sigma_\phi - \sigma_\theta|,\ |\sigma_\theta|\}\\ \varepsilon_{ec} &= \frac{2}{3}\mathrm{Max}\{|2\varepsilon_{\phi c} + \varepsilon_{\theta c}|,\ |\varepsilon_{\phi c} - \varepsilon_{\theta c}|,\ |2\varepsilon_{\theta c} + \varepsilon_{\phi c}|\}\end{aligned}\right\} \quad \text{(Tresca-Tresca)} \tag{1.12}$$

● Tresca-Tresca theory

$$\left.\begin{aligned}&\dot{\varepsilon}_{\phi c} = c\,\mathrm{sign}\,\sigma_\phi,\quad \dot{\varepsilon}_{\theta c} = 0 \quad (|\sigma_\phi| > |\sigma_\theta|)\\ &\dot{\varepsilon}_{\phi c} = 0,\quad \dot{\varepsilon}_{\theta c} = c\,\mathrm{sign}\,\sigma_\theta \quad (|\sigma_\theta| > |\sigma_\phi|)\end{aligned}\right\} \tag{1.13a}$$

$$\sigma_\phi\sigma_\theta < 0 \quad \dot{\varepsilon}_{\phi c} = c\,\mathrm{sign}\,\sigma_\phi,\quad \dot{\varepsilon}_{\theta c} = c\,\mathrm{sign}\,\sigma_\theta \tag{1.13b}$$

where the value of c is given by

$$c = mA^{1/m}\sigma_e^{n/m}\varepsilon_{ec}^{(m-1)/m} \quad \text{(strain-hardening)} \tag{1.14a}$$

$$c = mA\sigma_e^n t^{m-1} \quad \text{(time-hardening)} \tag{1.14b}$$

and σ_e, ε_{ec} are

$$\left.\begin{aligned}\sigma_e &= \mathrm{Max}\{|\sigma_\phi|,\ |\sigma_\phi-\sigma_\theta|,\ |\sigma_\theta|\}\\ \varepsilon_{ec} &= \frac{1}{2}\mathrm{Max}\{|2\varepsilon_{\phi c}+\varepsilon_{\theta c}|,\ |\varepsilon_{\phi c}-\varepsilon_{\theta c}|,\ |2\varepsilon_{\theta c}+\varepsilon_{\phi c}|\}\end{aligned}\right\} \tag{1.15}$$

The creep rates involved in (1.4) and (1.6) can be thus calculated from the relations (1.10) through (1.15) provided the values of stress and creep strain are specified at the relevant instant.

2.1.2. Governing equations in terms of rate of displacement

The substitution of (1.6) into (1.1) provides the following simultaneous linear differential equations with respect to $\dot{v}$ and $\dot{w}$:

$$\left.\begin{aligned}&\frac{d}{d\phi}\left\{r_0\left(K_{11}\dot{v}+K_{12}\frac{d\dot{v}}{d\phi}+K_{13}\dot{w}+K_{14}\frac{d\dot{w}}{d\phi}+K_{15}\frac{d^2\dot{w}}{d\phi^2}\right)\right\}-\frac{1}{r_1}\frac{d}{d\phi}\left\{r_0\left(L_{11}\dot{v}+L_{12}\frac{d\dot{v}}{d\phi}\right.\right.\\ &\left.\left.+L_{13}\dot{w}+L_{14}\frac{d\dot{w}}{d\phi}+L_{15}\frac{d^2\dot{w}}{d\phi^2}\right)+\cos\phi\left\{(L_{21}-r_1K_{21})\dot{v}+(L_{22}-r_1K_{22})\frac{d\dot{v}}{d\phi}\right.\right.\\ &\left.\left.+(L_{23}-r_1K_{23})\dot{w}+(L_{24}-r_1K_{24})\frac{d\dot{w}}{d\phi}+(L_{25}-r_1K_{25})\frac{d^2\dot{w}}{d\phi^2}\right\}\right.\\ &\qquad=Yr_0r_1-\frac{d}{d\phi}(\dot{P}_1r_0)+\frac{1}{r_1}\frac{d}{d\phi}(\dot{Q}_1r_0)-\cos(\dot{Q}_2-\dot{P}_2r_1)\\ &\left(\frac{r_0}{r_1}K_{11}+K_{21}\sin\phi\right)\dot{v}+\left(\frac{r_0}{r_1}K_{12}+K_{22}\sin\phi\right)\frac{d\dot{v}}{d\phi}+\left(\frac{r_0}{r_1}K_{13}+K_{23}\sin\phi\right)\dot{w}\\ &+\left(\frac{r_0}{r_1}K_{14}+K_{24}\sin\phi\right)\frac{d\dot{w}}{d\phi}+\left(\frac{r_0}{r_1}K_{15}+K_{25}\sin\phi\right)\frac{d^2\dot{w}}{d\phi^2}\\ &+\frac{1}{r_1}\frac{d}{d\phi}\left[\frac{1}{r_1}\frac{d}{d\phi}\left\{r_0\left(L_{11}\dot{v}+L_{12}\frac{d\dot{v}}{d\phi}+L_{13}\dot{w}+L_{14}\frac{d\dot{w}}{d\phi}+L_{15}\frac{d^2\dot{w}}{d\phi^2}\right)\right\}\right.\\ &\left.-\cos\phi\left\{L_{21}\dot{v}+L_{22}\frac{d\dot{v}}{d\phi}+L_{23}\dot{w}+L_{24}\frac{d\dot{w}}{d\phi}+L_{25}\frac{d^2\dot{w}}{d\phi^2}\right\}\right]\\ &\qquad=Zr_0-\left(\frac{r_0}{r_1}\dot{P}_1+\dot{P}_2\sin\phi\right)-\frac{1}{r_1}\frac{d}{d\phi}\left\{\frac{1}{r_1}\frac{d}{d\phi}(\dot{Q}_1r_0)-\dot{Q}_2\cos\phi\right\}\end{aligned}\right\} \tag{1.16}$$

The boundary condition of the above equations are, for example,

Center: $$\phi=0,\ \dot{v}=\frac{d^2\dot{v}}{d\phi^2}=\frac{d\dot{w}}{d\phi}=0 \tag{1.17a}$$

Clamped edge: $$\phi=\beta,\ \dot{v}=\dot{w}=\frac{d\dot{w}}{d\phi}=0 \tag{1.17b}$$

Simply supported edge: $$\phi=\beta,\ \dot{v}=\dot{w}=\dot{M}_\phi=0 \tag{1.17c}$$

In order to determine the states of stress and deformation for the given shell, it is necessary to obtain the solution of (1.16) at every stage of deformation. Since it is difficult to solve (1.16) analytically, we calculate them numerically by the method of finite-difference.

If the mesh points of difference interval $g=\beta/N$ (N is the number of division over the semi-angle β) are superimposed on a meridian section of the shell, and the derivatives with respect to ϕ are replaced by the usual centered difference[24], the equations (1.16) together with (1.17) are reduced to the following simultane-

ous linear equations concerning $\dot{v}_i$ and $\dot{w}_i$ (the values of $\dot{v}$ and $\dot{w}$ at the mesh point i):

$$\boldsymbol{A}\boldsymbol{X}=\boldsymbol{B} \tag{1.18}$$

Here, A, X and B denote the coefficient matrix, the unknown column vector and the inhomogeneous column vector, the expressions of which will be given by specifying the geometry of the shell. Since the matrix A is constant with respect to time, $X(t)$ at any instant can be obtained by multiplying $B(t)$ at that instant by the inverse of A, provided that it has been evaluated at the beginning of the calculation. The errors caused by the centered difference are of the order of g^2. Integrals appearing in (1.7) are carried out numerically according to Simpson's 1/3 rule[25] by dividing the thickness of the shell into N' equidistant portions (in the present paper N' is assumed to be 10 throughout). The errors due to the numerical integration are proportinal to $(1/N')^6$ which are much smaller than those of the finite-difference.

2.2. Governing equations for pressurised circular cylindrical shells[1)~4)]

Let's consider first a pressurised circular cylindrical shell shown in Fig. 1.2. In the present case, the meridians are reduced to a family of generators of the cylinder and the external force corresponding to internal pressure are represented by $Z=-p$. Hence, the relations for the present shell can be directly obtained by the replacements

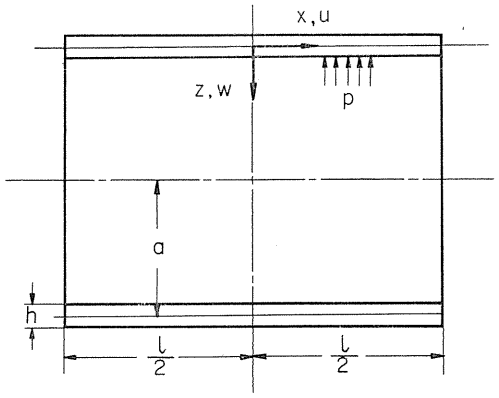

FIG. 1.2. Circular cylindrical shell subjected to internal pressure.

$$\left.\begin{aligned} &\phi=\frac{\pi}{2},\quad r_0=r_2=a,\quad r_1 d\phi=dx,\quad r=\infty \\ &Y=0,\quad Z=-p \end{aligned}\right\} \tag{1.19}$$

If we employ the non-dimensional quantities defined previously and replace the derivatives by the corresponding finite-difference, the governing equations of the pressurised circular cylindrical shells are obtained. Since the details of the equations are reported already[1)~4)], they will be omitted here for the sake of brevity.

For long thin circular cylindrical shell, in particular, the state of deformation in their middle portion is uniform in axial direction. Such a portion may be treated as a long thin circular tube, and exact solutions in the closed form can be obtained. For the cylinder with closed ends, for example, the components of stress is given by

$$S_x = \frac{1}{2}, \quad S_0 = 1 \tag{1.20}$$

Then, the deflection at time t are:

- Mises-Mises theory

$$W = -\left\{\left(1-\frac{1}{2}\nu\right)+\left(\frac{3}{4}\right)^{(n+1)/2}(EA)\left(\frac{\hat{p}a}{h}\right)^{n-1}t^m\right\} \tag{1.21 a}$$

- Tresca-Mises theory

$$W = -\left\{\left(1-\frac{1}{2}\nu\right)+\left(\frac{3}{4}\right)(EA)\left(\frac{\hat{p}a}{h}\right)^{n-1}t^m\right\} \tag{1.21 b}$$

- Tresca-Tresca theory

$$W = -\left\{\left(1-\frac{1}{2}\nu\right)+(EA)\left(\frac{\hat{p}a}{h}\right)^{n-1}t^m\right\} \tag{1.21 c}$$

2.3. Governig equations for pressurised spherical shells

The basic relations for a spherical shell under internal pressure (Fig. 1.3) can be directly obtained by applying the replacements

$$r_1 = r_2 = a, \quad r_0 = a\sin\phi, \quad Y = 0, \quad Z = -p \tag{1.22}$$

to the preceding relations for general shells. If the resulting relations are re-written by using the non-dimensional quantities defined previously, the governing equations for the present problem are reduced to as follows:

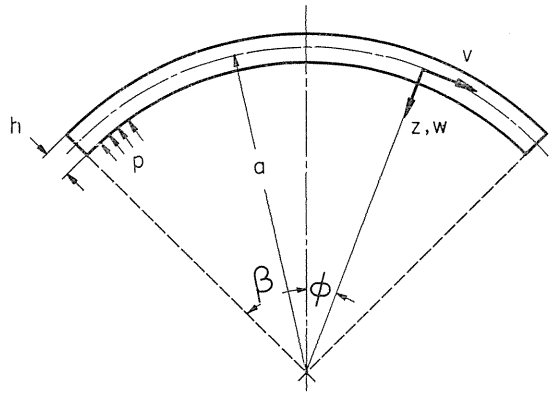

Fig. 1.3. Spherical shell subjected to internal pressure.

$$\left.\begin{aligned}&\frac{d}{d\phi}\{(n_\phi - Hm_\phi)\sin\phi\} - (n_\theta - Hm_\theta)\cos\phi = 0\\&\frac{d^2}{d\phi^2}(n_\phi\sin\phi) - \frac{d}{d\phi}(n_\theta\cos\phi) + (n_\phi + n_\theta - 2)\sin\phi = 0\end{aligned}\right\} \tag{1.23}$$

$$\left.\begin{aligned}&\phi = 0,\ \dot{V} = \frac{d^2\dot{V}}{d\phi^2} = \frac{d\dot{W}}{d\phi} = 0 \qquad \text{(center)}\\&\phi = \beta,\ \dot{V} = \dot{W} = \frac{d\dot{W}}{d\phi} = 0 \qquad \text{(clamped edge)}\\&\phi = \beta,\ \dot{V} = \dot{W} = \dot{m}_\phi = 0 \qquad \text{(simply supported edge)}\end{aligned}\right\} \tag{1.24}$$

$$\left.\begin{aligned}\dot{S}_\phi = \frac{1}{1-\nu^2}\Big[&\Big\{\Big(\frac{d\dot{V}}{d\phi} - \dot{W}\Big) - \frac{1}{2}H\eta\frac{d}{d\phi}\Big(\dot{V} + \frac{d\dot{W}}{d\phi}\Big)\Big\}\\&+ \nu\Big\{(\dot{V}\cot\phi - \dot{W}) - \frac{1}{2}H\eta\cot\phi\Big(\dot{V} + \frac{d\dot{W}}{d\phi}\Big)\Big\} - (\dot{E}_{\phi c} + \nu\dot{E}_{\theta c})\\\dot{S}_\theta = \frac{1}{1-\nu^2}\Big[&\nu\Big\{\Big(\frac{d\dot{V}}{d\phi} - \dot{W}\Big) - \frac{1}{2}H\eta\frac{d}{d\phi}\Big(\dot{V} + \frac{d\dot{W}}{d\phi}\Big)\Big\}\\&+ \Big\{(\dot{V}\cot\phi - \dot{W}) - \frac{1}{2}H\eta\cot\phi\Big(\dot{V} + \frac{d\dot{W}}{d\phi}\Big)\Big\} - (\dot{E}_{\theta c} + \nu\dot{E}_{\phi c})\end{aligned}\right\} \tag{1.25}$$

$$\dot{n}_\phi = \frac{1}{2}\int_{-1}^{1}\dot{S}_\phi d\eta,\quad \dot{n}_\theta = \frac{1}{2}\int_{-1}^{1}\dot{S}_\theta d\eta \tag{1.26}$$

$$\dot{m}_\phi = \frac{1}{4}\int_{-1}^{1}\dot{S}_\phi\eta d\eta,\quad \dot{m}_\theta = \frac{1}{4}\int_{-1}^{1}\dot{S}_\theta\eta d\eta \tag{1.27}$$

● Mises-Mises and Tresca-Mises theories

$$\left.\begin{aligned}\dot{E}_{\phi c} &= m(EA)^{1/m}\Big(\frac{\hat{p}a}{2h}\Big)^{(n-1)/m}S_e{}^{(n-m)/m}E_{ec}{}^{(m-1)/m}\Big(S_\phi - \frac{1}{2}S_\theta\Big)\\\dot{E}_{\theta c} &= m(EA)^{1/m}\Big(\frac{\hat{p}a}{2h}\Big)^{(n-1)/m}S_e{}^{(n-m)/m}E_{ec}{}^{(m-1)/m}\Big(S_\theta - \frac{1}{2}S_\phi\Big)\end{aligned}\right\} \text{(strain-hardening)} \tag{1.28 a}$$

$$\left.\begin{aligned}\dot{E}_{\phi c} &= m(EA)\Big(\frac{\hat{p}a}{2h}\Big)^{n-1}S_e{}^{n-1}t^{m-1}\Big(S_\phi - \frac{1}{2}S_\theta\Big)\\\dot{E}_{\theta c} &= m(EA)\Big(\frac{\hat{p}a}{2h}\Big)^{n-1}S_e{}^{n-1}t^{m-1}\Big(S_\theta - \frac{1}{2}S_\phi\Big)\end{aligned}\right\} \text{(time-hardening)} \tag{1.28 b}$$

where

$$\left.\begin{aligned}S_e &= (S_\phi^2 - S_\phi S_\theta + S_\theta^2)^{1/2}\\E_{ec} &= \frac{2}{\sqrt{3}}(E_{\phi c}^2 + E_{\phi c}E_{\theta c} + E_{\theta c}^2)^{1/2}\end{aligned}\right\} \text{(Mises-Mises)} \tag{1.29 a}$$

$$\left.\begin{aligned}S_e &= \mathrm{Max}\{|S_\phi|,\ |S_\phi - S_\theta|,\ |S_\theta|\}\\E_{ec} &= \frac{2}{3}\mathrm{Max}\{|2E_{\phi c} + E_{\theta c}|,\ |E_{\phi c} - E_{\theta c}|,\ |2E_{\theta c} + E_{\phi c}|\}\end{aligned}\right\} \text{(Tresca-Mises)} \tag{1.29 b}$$

● Tresca-Tresca theory

$$\left.\begin{aligned} S_\phi S_\theta > 0 \quad & \dot{E}_{\phi c} = C \operatorname{sign} S_\phi,\ \dot{E}_{\theta c} = 0 \quad (|S_\phi| > |S_\theta|) \\ & \dot{E}_{\phi c} = 0,\ \dot{E}_{\theta c} = C \operatorname{sign} S_\theta \quad (|S_\theta| > |S_\phi|) \end{aligned}\right\} \tag{1.30 a}$$

$$S_\phi S_\theta < 0 \quad \dot{E}_{\phi c} = C \operatorname{sign} S_\phi,\ \dot{E}_{\theta c} = C \operatorname{sign} S_\theta \tag{1.30 b}$$

where

$$C = m(EA)^{1/m}\left(\frac{\hat{p}a}{2h}\right)^{(n-1)/m} S_e^{\,n/m} E_{ec}^{\,(m-1)/m} \quad \text{(strain-hardening)} \tag{1.31 a}$$

$$C = m(EA)\left(\frac{\hat{p}a}{2h}\right)^{n-1} S_e^{\,n} t^{m-1} \quad \text{(time-hardening)} \tag{1.31 b}$$

$$\left.\begin{aligned} & S_e = \operatorname{Max}\{|S_\phi|,\ |S_\phi - S_\theta|,\ |S_\theta|\} \\ & E_{ec} = \frac{1}{2}\operatorname{Max}\{|2E_{\phi c} + E_{\theta c}|,\ |E_{\phi c} - E_{\theta c}|,\ |2E_{\theta c} + E_{\phi c}|\} \end{aligned}\right\} \tag{1.32}$$

By replacing the derivatives with the corresponding finite-difference and proceeding analogously as before, we readily obtain the governing equations for pressurised spherical shells.

In the case of a complete sphere, especially, solutions of closed form may be easily obtained. The components of radial displacement, for example, are furnished by the following relation independently of the type of the creep theory:

$$W = -\left\{(1-\nu) + \frac{1}{2}(EA)\left(\frac{\hat{p}a}{h}\right)^{n-1} t^m\right\} \tag{1.33}$$

3. Method of Calculation

The first step of the calculation is to determine the elastic deformation corresponding to the given pressure, which provides the initial condition of the succeeding calculation. The fundamental equations for elastic state may be obtained by (1.1) through (1.18) only if the terms connected to the creep rates are replaced by 0 and dots on every symbol are excluded.

Then creep rate at a certain instant can be calculated by relations (1.10) through (1.15) from the values of stres and creep strain at that instant. Then, $\dot{v}_i$ and $\dot{w}_i$ are determined by (1.16) and (1.17). The rates of the other variables are furnished by the relations (1.3) through (1.7) together with these values. Hence, the variables at the succeeding instants can be determined by integrating numerically the rates of variables thus obtained with respect to time.

At the particular instant $t=0$ (i.e. $\varepsilon_{ec}=0$), however, creep rate becomes infinity as can be seen from (1.10) through (1.15). Then, the above mentioned procedure for creep state cannot be applied. To avoid this difficulty, we select a particular short interval $0 \leqq t \leqq t_0$ just after the loading, and calculate the increments of variables during this interval by integrating fundamental relations instead of calculating their rates. If the variation of stress during this interval is sufficiently small by comparison with the values of stress at instant $t=0$ and the state of stress can be assumed to be constant during the interval, creep strain increments may be calculated by integrating (1.10) and (1.13) to be expressed as follows independently of the hardening-hypotheses:

● Mises-Mises and Tresca-Mises theories

$$\Delta\varepsilon_{\phi c}=A\sigma_e^{n-1}(\Delta t)^m\left(\sigma_\phi-\frac{1}{2}\sigma_\theta\right),\quad \Delta\varepsilon_{\theta c}=A\sigma_e^{n-1}(\Delta t)^m\left(\sigma_\theta-\frac{1}{2}\sigma_\phi\right) \tag{1.34}$$

where

$$\sigma_{e0}=(\sigma_{\phi 0}^2-\sigma_{\phi 0}\sigma_{\theta 0}+\sigma_{\phi 0}^2)^{1/2} \quad \text{(Mises-Mises)} \tag{1.35a}$$

$$\sigma_{e0}=\mathrm{Max}\{|\sigma_{\phi 0}|,\ |\sigma_{\phi 0}-\sigma_{\theta 0}|,\ |\sigma_{\theta 0}|\} \quad \text{(Tresca-Mises)} \tag{1.35b}$$

● Tresca-Tresca theory (*e.g.* in the case of $\sigma_{\phi 0}>\sigma_{\theta 0}>0$)

$$\Delta\varepsilon_{\phi c}=A\sigma_{e0}^n(\Delta t)^m,\quad \Delta\varepsilon_{\theta c}=0 \tag{1.36}$$

where

$$\sigma_{e0}=\mathrm{Max}\{|\sigma_{\phi 0}|,\ |\sigma_{\phi 0}-\sigma_{\theta 0}|,\ |\sigma_{\theta 0}|\} \tag{1.37}$$

In the above relations $\sigma_{\phi 0}$ and $\sigma_{\theta 0}$ denote the initial value of stress. Other relations, *i.e.* (1.4), (1.6), (1.16) and (1.17), must be also integrated with respect to time, but they remain formally unchanged. Thus, increments of variables can be calculated from (1.4) to (1.17) by the same procedures as mentioned above only if the relations (1.10) to (1.15) are replaced by (1.34) through (1.37). In the following calculation, the value of $t_0=10^{-5}$ hr was ascertained to be satisfactory enough for this purpose.

Numerical integration of the above mentioned rates of variables with respect to time was performed by the Runge-Kutta-Gill method[25].

4. Results of Calculation and Discussion

As a numerical example, the following two cases are considered for simply supported circular cylindrical shells with closed ends of 0.15 per cent carbon steel at 450°C. As the first example, the creep behaviour of shells of $\alpha=\pi$ and $\alpha=2\pi$ under four kinds of constant load between $pa/h=5$ and 20 kg/mm^2 are calculated according to the three kinds of creep theories. The creep of shells of $\alpha=2\pi$ subjected to the step-wisely varying load among $pa/h=7.5$, 10, 12.5 and 15 kg/mm^2 according to the Mises-Mises theory is selected as the second example. The shells of $\alpha=\pi$ and 2π correspond to short and long ones respectively[21], and pa/h is equivalent to the hoop stress in long thin circular tubes.

Material constants employed are

$$E=18{,}000\ \text{kg/mm}^2,\ \nu=0.3$$

$$A=4.36\times10^{-7}\ (\text{kg/mm}^2)^{-4.66}\,(\text{hr})^{-0.218},\ m=0.218,\ n=4.66$$

which were obtained by a creep test for the above mentioned carbon steel.

The truncation errors due to the replacement of the derivative by the centered difference is the order of g^2, where $g=1/N$[24]. However, difference between numerical results obtained in the case of $g=1/25$ and $g=1/50$ is less than 0.2 per cent for a cylindrical shell of $\alpha=2\pi$, $pa/h=15$ kg/mm^2. Hence the lattice interval of $g=1/25$ is practically admissble and is employed in the following calculation.

The errors of the numerical integration due to the Ruge-Kutta-Gill method, on the other hand, are in proportion to $(\Delta t)^5$ (Δt; increment of time)[25], and are

much smaller than those involved in finite-difference mentioned above. In the present calculation, the value of Δt is specified so that W at $\xi=0$ may increase by a certain constant fraction (*i.e.*, $1/K$) of the initial elastic value of W at $\xi=0$ during the interval Δt. The results of the calculation for $K=30$ and $K=60$ were ascertained to coincide with each other to an accuracy of six significant figures in the case of $g=1/25$, $\alpha=2\pi$ and $pa/h=15$ kg/mm^2. The following calculation, therefore, are all performed by using the value $K=30$.

When the creep deformation proceeds sufficiently far and creep strain becomes large enough in comparison with elastic one, the rate of stress decreases gradually and its distribution tends to that of steady-state ceeep. In the present analysis, therefore, the calculation is carried on up to the state Max $\left|\frac{\dot{\sigma}}{\sigma}\right|<10^{-7}$ (hr)$^{-1}$ and the resulting stress is regarded as that of steady-state (*i.e.*, $t=\infty$). These results are entered into the subsequent figures. According to the results due to the Mises-Mises theory for $pa/h=20$ kg/mm^2, for example, the above condition is satisfied at about $t=6{,}000$ and 4,000 hr in case of $\alpha=\pi$ and $\alpha=2\pi$, respectively, and ratios between creep strain and elastic strain at these instants are less than about 20 and 15 for these parameters.

The above procedures were programmed according to Fortran IV, and calculations were all carried out in double precision (13 digits) by using HITAC-5020. The programme consists of about 71,000 machine words (in case of $g=1/25$), and the time of calculation was, for example, about 150 sec in case of the following shell of $\alpha=2\pi$, $pa/h=15$ kg/mm^2 due to the Mises-Mises theory and the strain-hardening hypothesis in the time ragne of $t=0\sim120$ hr.

4.1. Circular cylindrical shells under constant internal pressure

4.1.1. Mises-Mises theory[1)-4)]

Numerical results due to the Mises-Mises theory for constant pressure are shown in Table 1.1 and Figs. 1.4 to 1.10. The solid and the dashed line in these figures are the results of the strain-hardening and the time-hardening hypothesis, respectively. In the following, the internal pressure p is employed as the reference pressure $\hat{p}$ in the definition of non-dimensional variables. Figs. 1.4 and 1.5 show the variation of maximum deflection and the maximum stress for various values of pa/h. Open circles on the ordinate in these figures represent the values corresponding to the elastic deformation. In Fig. 1.4 (a), (b), the difference between the results of both hypotheses is less than about 5 per cent. Fig. 1.5 (a), (b) shows $(\sigma_\theta)_{\max}h/pa$ which occurs on the surface $z/h=-1$ at $2x/l=0.4$ to 0 and 0.7 to 0.6, respectively. The change of the location of these maximum stress with the lapse of time may be estimated approximately by Figs. 1.7 and 1.8 below, together with the fact that M_θ/pah shows almost the same distribution as M_x/pah but is one-third to one-ninth times the latter in magnitude.

Closed circles on the ordinate in these figures show the maximum stress at steady-state creep. It will be observed that the maximum stresses in the cylindrical shell of $\alpha=\pi$ and 2π are about 5 and 3 per cent larger even in the steady-state than those of long thin circular tube in which the relation $\sigma_\theta h/pa=1.0$ holds always. The dependence of rate of decrease of $(\sigma_\theta)_{\max}h/pa$ on the magnitude of internal pressure and the geometry of shells will be also observed in these figures. The difference between the solid and dashed lines in Fig. 1.4 are less than 0.5 per

TABLE 1.1. Computed values of $Ehw_{\max}/pa^2$, $Ehu_{\max}/pal$, $(M_x)_{\max}/pah$, $(M_\theta)_{\max}/pah$ and $(N_\theta)_{\max}/pa$ at several instants

(a) $\alpha=\pi$, $pa/h=15$ kg/mm^2

t (hr)		0	0.1	1	10	100	∞
$Ehw_{\max}/pa^2$	S	−0.923	−1.473	−1.815	−2.369	−3.273	—
	T		−1.484	−1.835	−2.403	−3.324	
$Ehw_{\max}/pal$	S	0.1201	0.1234	0.1256	0.1299	0.1378	—
	T		0.1234	0.1254	0.1290	0.1358	
$(M_x)_{\max}/pah$	S	−0.0818	−0.0662	−0.0610	−0.0559	−0.0517	−0.0454
	T		−0.0644	−0.0583	−0.0527	−0.0486	
$(M_\theta)_{\max}/pah$	S	−0.0246	−0.0129	−0.0103	−0.0088	−0.0077	−0.0054
	T		−0.0116	−0.0084	−0.0059	−0.0057	
$(N_\theta)_{\max}/pa$	S	1.073	1.057	1.051	1.046	1.042	1.036
	T		1.055	1.049	1.043	1.039	

S: strain-hardening hypothesis
T: time-hardening hypothesis

(b) $\alpha=2\pi$, $pa/h=15$ kg/mm^2

t (hr)		0	0.1	1	10	100	∞
$Ehw_{\max}/pa^2$	S	−0.905	−1.392	−1.699	−2.201	−3.027	—
	T		−1.400	−1.712	−2.221	−3.057	
$Ehu_{\max}/pal$	S	0.1100	0.1121	0.1133	0.1157	0.1202	—
	T		0.1122	0.1140	0.1155	0.1193	
$(M_x)_{\max}/pah$	S	−0.0822	−0.0678	−0.0629	−0.0577	−0.0537	−0.0483
	T		−0.0661	−0.0587	−0.0552	−0.0514	
$(M_\theta)_{\max}/pah$	S	−0.0247	−0.0131	−0.0105	−0.0091	−0.0080	−0.0058
	T		−0.0012	−0.0077	−0.0064	−0.0061	
$(N_\theta)_{\max}/pa$	S	1.055	1.033	1.029	1.025	1.022	1.018
	T		1.031	1.026	1.022	1.020	

S: strain-hardening hypothesis
T: time-hardening hypothesis

cent.

Fig. 1.6 is the distribution of Ehw/pa^2 in the case of $pa/h=15$ kg/mm^2. Curves of $t=0$ shows the elastic deflection at the instant of loading, and circles on the ordinate are the values calculated by equation (1.21 a) for $t=0$, 0.1, 1, 10 and 100 hr. Hence it will be observed that the deflection at the center of the shell of $\alpha=\pi$ are about 15 per cent larger than that of long thin circular tubes. In the shells of $\alpha=2\pi$, on the other hand, the circles coincide not only with the results of elastic solution but also with those of the creep solution due to the strain-hardening hypthesis within the accuracy of 1 per cent. According to the results for $\alpha=2\pi$, *e.g.*, Figs. 1.7 (b) and 1.8 (b), the central portion of the shell is almost in the state of hoop stress. Consequently, the fact that the results of exact solution (1.21 a) coincide with the corresponding numerical results confirms the

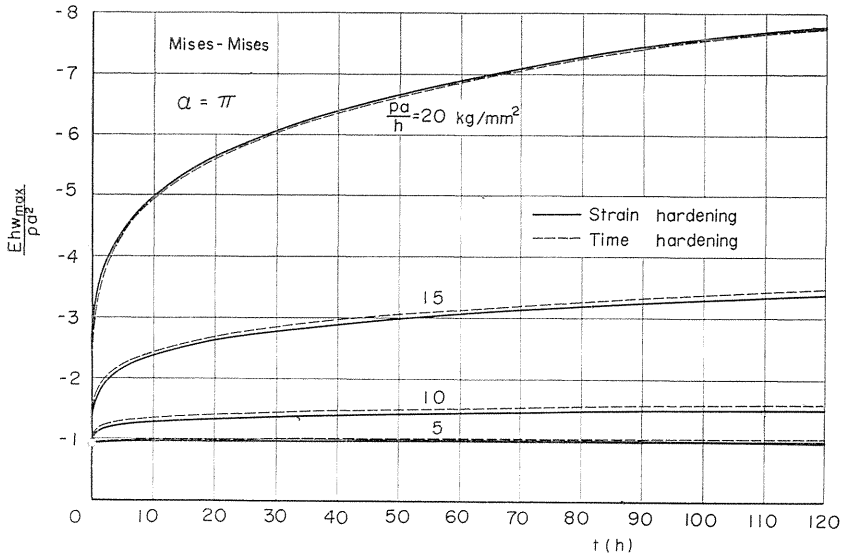

(a) $\alpha=\pi$

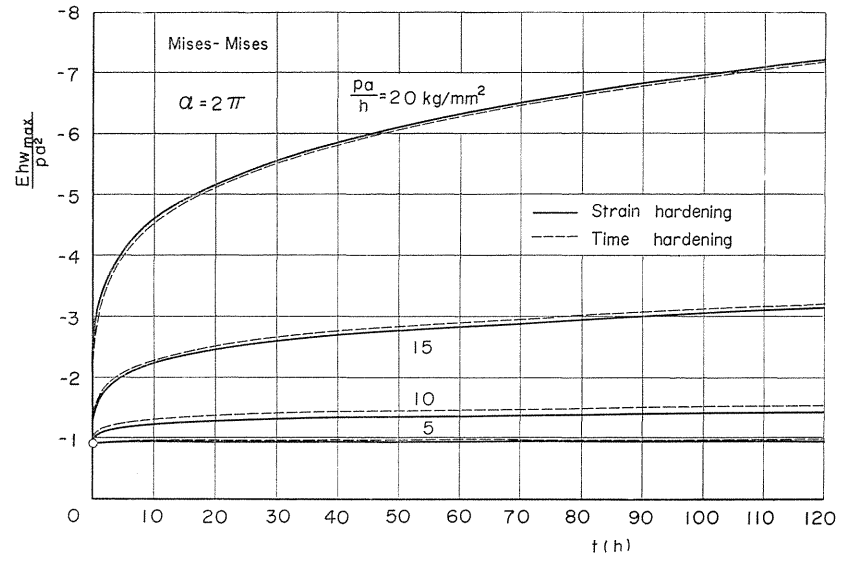

(b) $\alpha=2\pi$

FIG. 1.4. Variation of the maximum deflection.

accuracy of the present procedures. The maximum deflection in the shell of $\alpha=2\pi$ occurs at $2x/l=0.55$ to 0.65 and about 10 per cent larger than those calculated by (1.21 a). It should be noted that these portions of maximum deflection can not be neglected from the viewpoint of structural design.

Distribution of N_θ/pa and M_x/pah in case of $pa/h=15$ kg/mm^2 are shown in Figs. 1.7 and 1.8. The maximum values of N_θ/pa for $\alpha=\pi$ and 2π are about 4

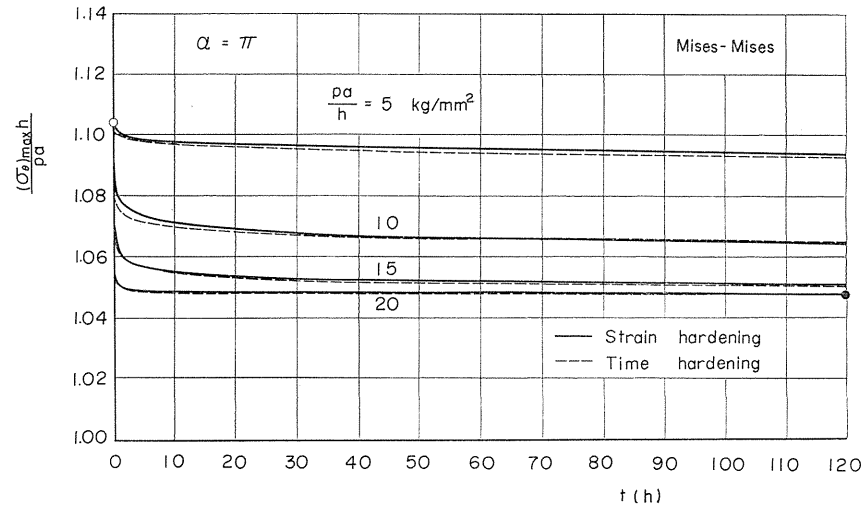

(a) $\alpha=\pi$

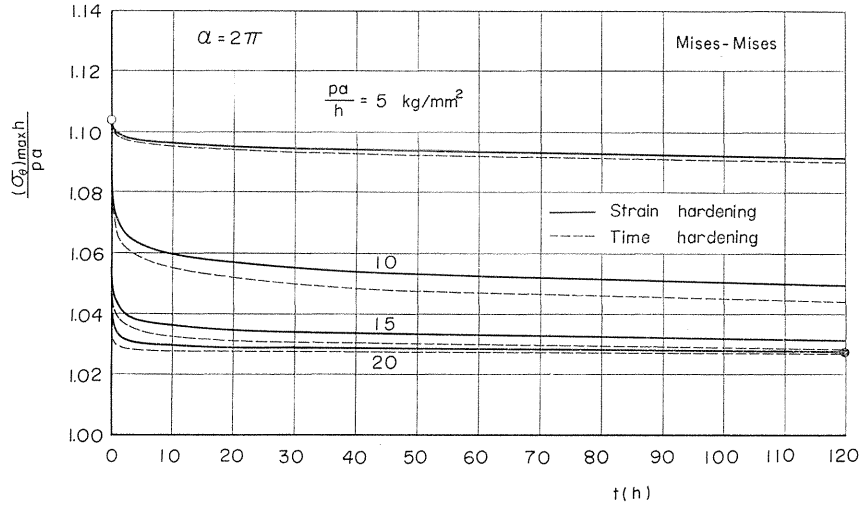

(b) $\alpha=2\pi$

FIG. 1.5. Variation of the maximum stress.

and 2 per cent larger even in the steady-state creep than the value $N_\theta/pa=1.0$ in long circular tubes. The value N_θ/pa does not vanish at $2x/l=1$ because of the effect of axial force. On the other hand, M_x/pah in Fig. 1.8 is significant only near the supported ends, and in particular it is almost negligible in the central portion of the shell of $\alpha=2\pi$. In the case of $n=1$, M_x/pah vanishes at $2x/l=0$ in the shell of $\alpha=\pi$, and at $2x/l=0$ and 0.5 in the shell of $\alpha=2\pi$[21]. Therefore, it should be observed that the effect of supported end prevails in wider region as the creep proceeds. The differences between solid and dashed lines in Figs. 1.7 and 1.8 are less than 3 and 6 per cent, respectively. It will be also observed that the changes in the distributions of the membrane force and bending moment

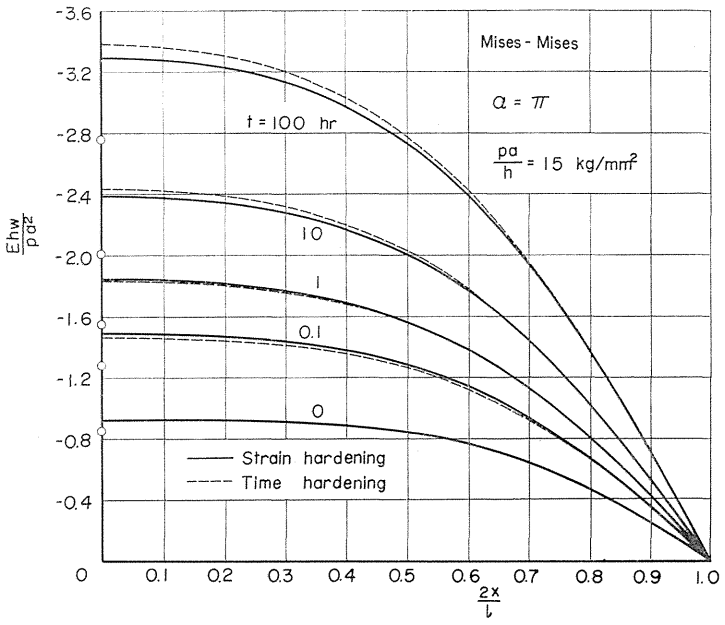

(a) $\alpha=\pi$

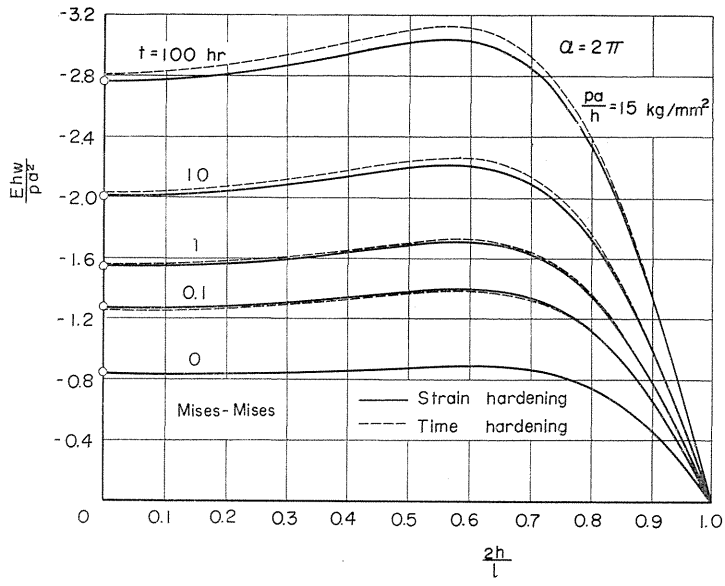

(b) $\alpha=2\pi$

Fig. 1.6. Distribution of the deflection.

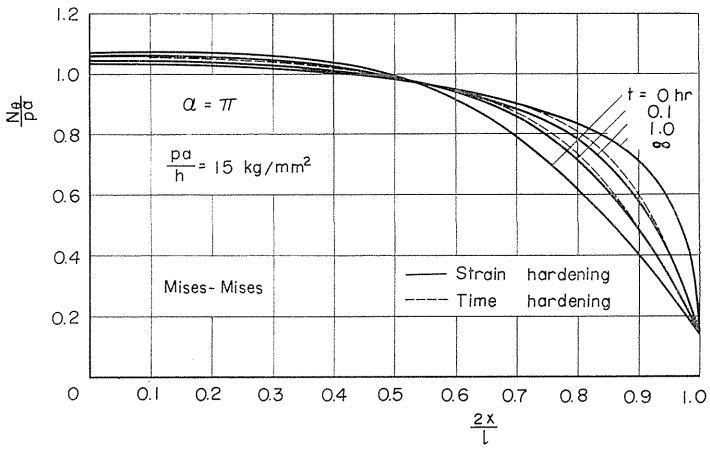

(a) $\alpha=\pi$

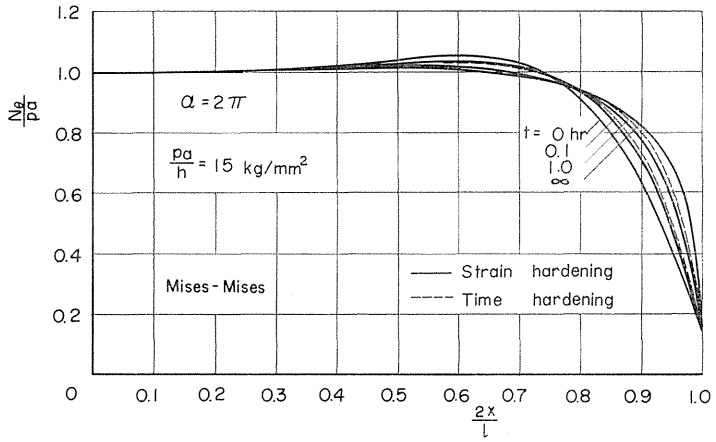

(b) $\alpha=2\pi$

FIG. 1.7. The circumferential component of the membrane force.

in these figures are quite rapid in the first few hours and their maximum values change within 10 hr by about 60 per cent of their total variations.

Finally Figs. 1.9 and 1.10 illustrate examples of the stress distribution in section $2x/l=0.8$. It should be noticed that the stress distribution in the section shows a remarkable tendency to become more uniform in a relatively short time.

4. 1. 2. Tresca-Mises and Tresca-Tresca theories[4]

Some of the numerical results for the shell of $\alpha=2\pi$ due to the Tresca-Mises and Tresca-Tresca theories are presented in Figs. 1.11 to 1.13.

Fig. 1.11 shows the distribution of deflection obtained by these two kinds of theory for the case of $pa/h=15$ kg/mm². The small circles on the ordinate again correspond to the rigorous solution for long thin circular tubes (1.21 b), (1.21 c). Though the results of the Tresca-Mises theory, Fig. 1.11 (a), show the similar

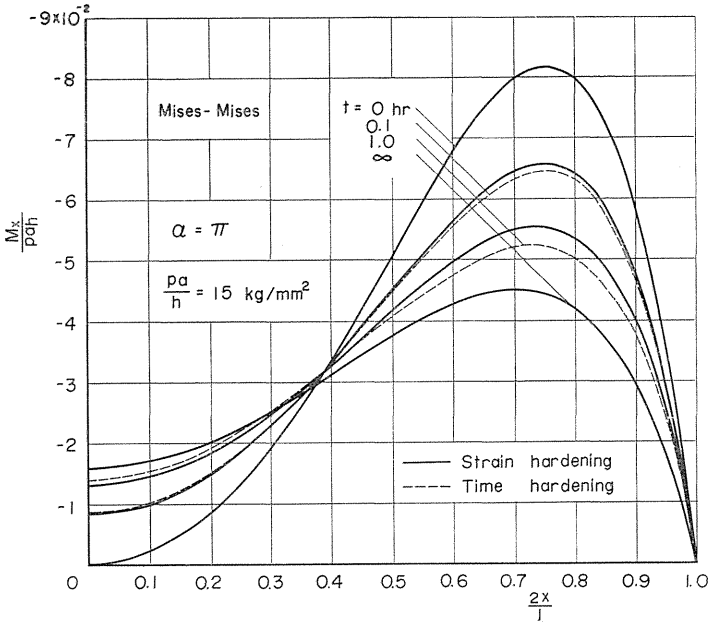

(a) $\alpha=\pi$

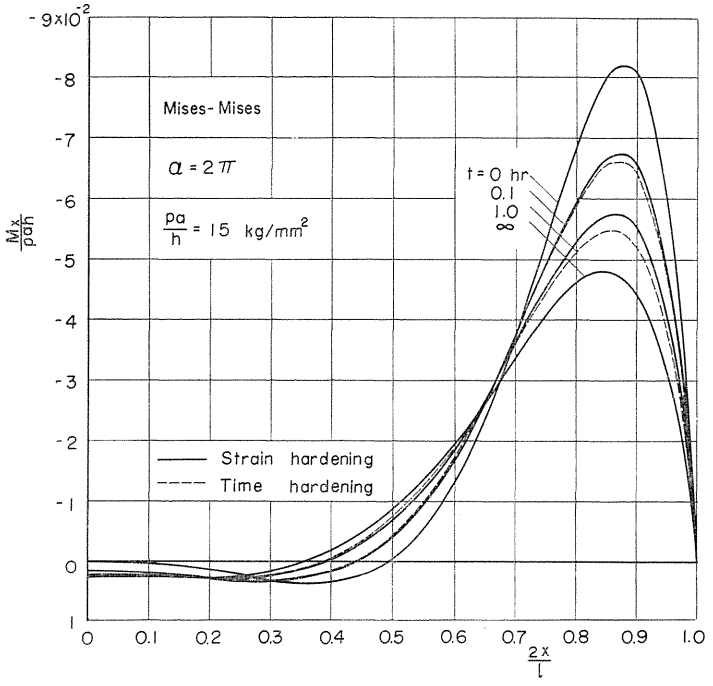

(b) $\alpha=2\pi$

FIG. 1.8. The axial component of the bending moment.

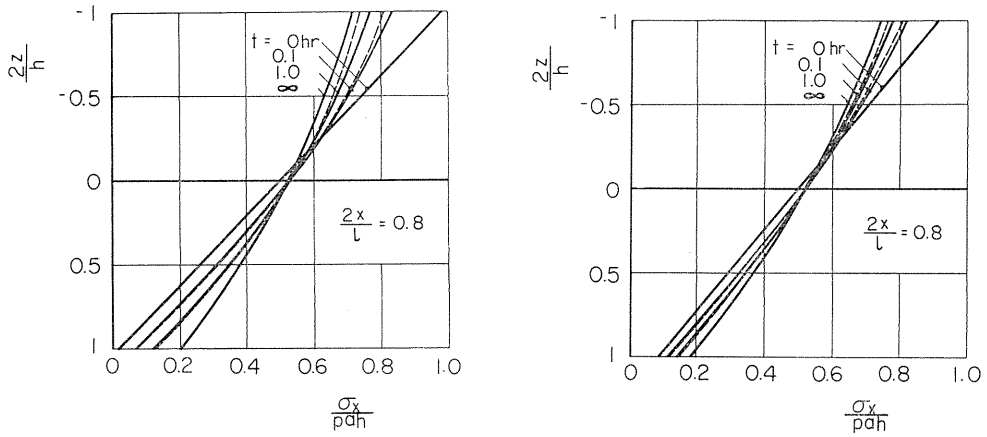

(a) $\alpha=\pi$, $pa/h=15$ kg/mm^2 (b) $\alpha=2\pi$, $pa/h=15$ kg/mm^2

FIG. 1.9. The axial component of the stress.

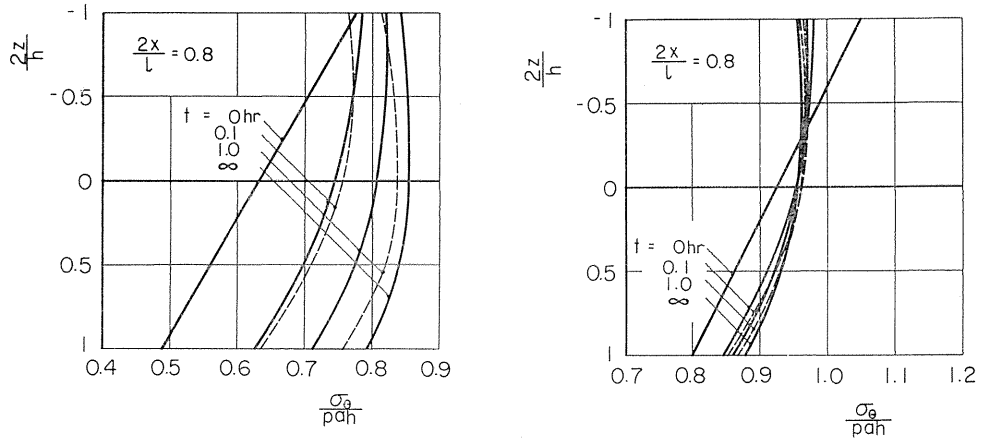

(a) $\alpha=\pi$, $pa/h=15$ kg/mm^2. (b) $\alpha=2\pi$, $pa/h=15$ kg/mm^2.

FIG. 1.10. The circumferential component of the stress.

distribution as those of the Mises-Mises theory, the values are about 40 per cent larger than those due to the latter theory. The difference between the strain-hardening and the time-hardening hypothesis is less than 2 per cent, and the values at the center nearly coincide with those of (1.21) for long tube.

In the results due to the Tresca-Tresca theory, on the other hand, the location of maximum deflection moves considerably with time, and the maximum value due to the strain-hardening hypothesis, especially, occurs at the center of the shell at the time $t=100$ hr. The difference between the solid and dashed lines are less than 3 per cent. Although the deflection of the center of shell coincides with the value of (1.21 c) for $t=0.1$, the difference between them increase with time thereafter. According to the Tresca-Tresca theory, therefore, the region which is influenced by the end condition increase as the creep deformation proceeds, and the distribution of deformation becomes alike to that of the shell of

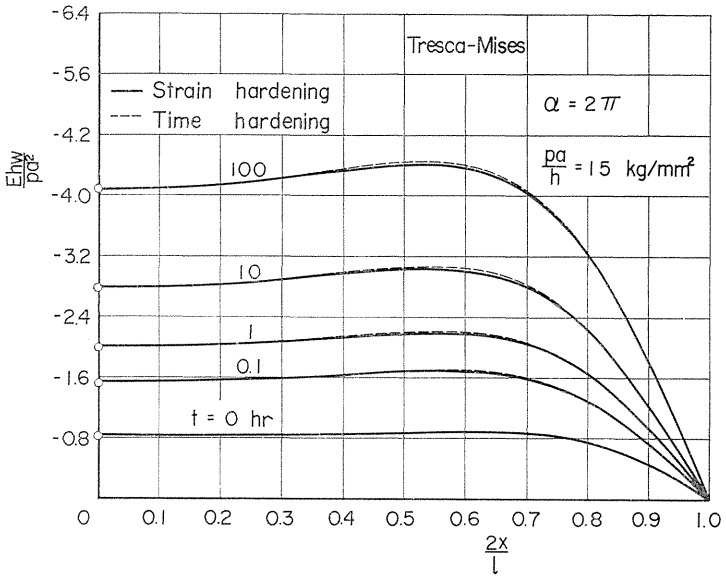

(a) Tresca-Mises

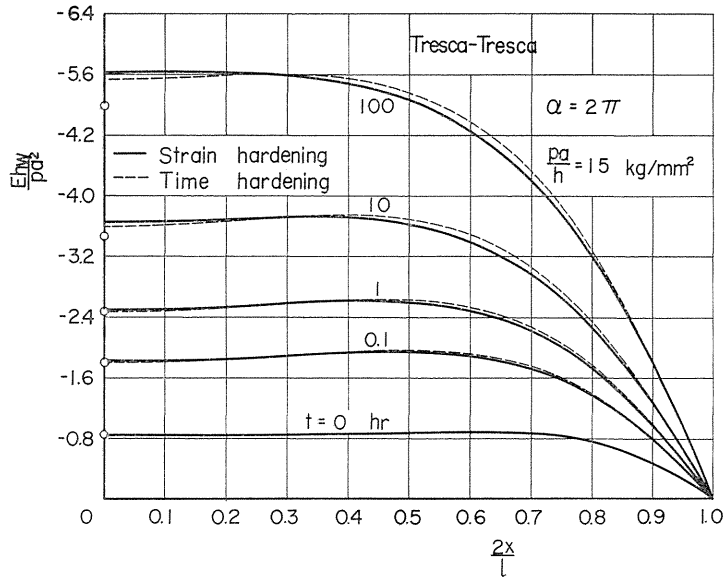

(b) Tresca-Tresca

FIG. 1.11. Distribution of the deflection.

$\alpha=\pi$ shown in Fig. 1.6 (a). The maximum value of deflection in this case is about 80 and 40 per cent larger than those of the Mises-Mises and the Tresca-Mises theory, respectively.

As regards the components of axial displacement, membrane force and bending moment, the Tresca-Mises theory was found to show the similar distribution

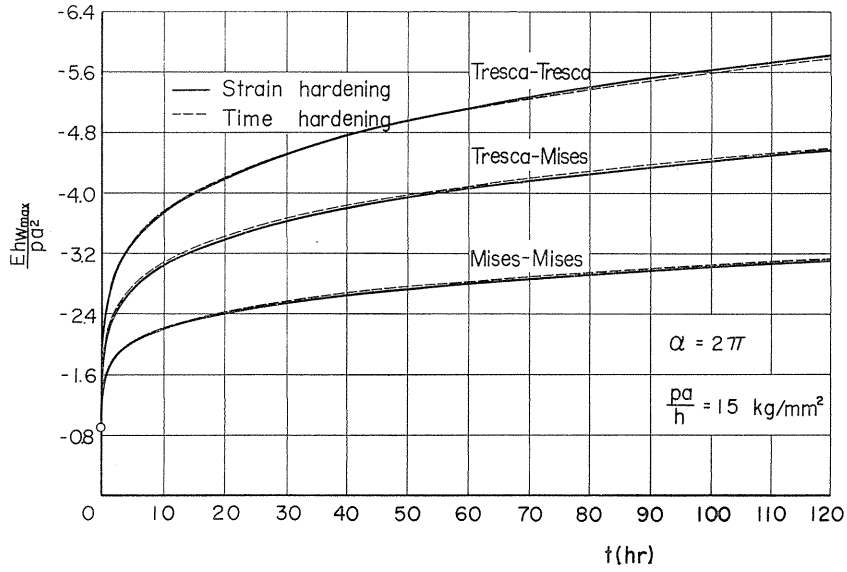

FIG. 1.12. Comparison of the variation of the maximum deflection.

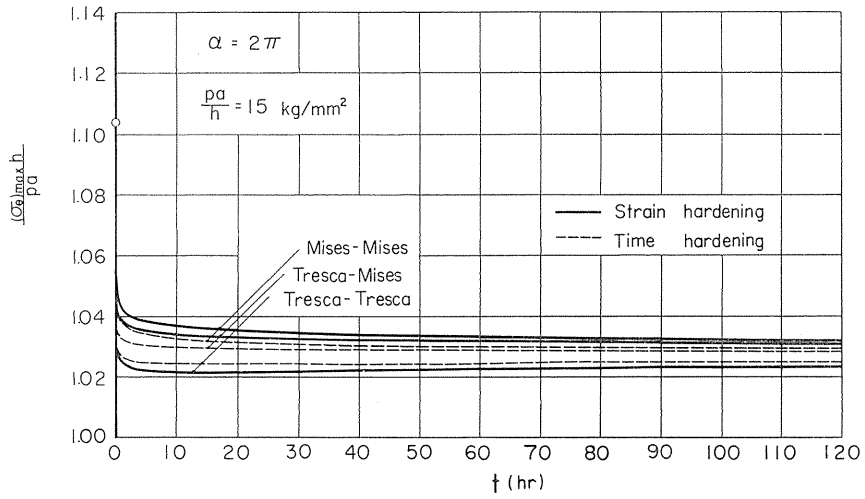

FIG. 1.13. Comparison of the variation of the maximum stress.

and nearly the same magnitude as in the case of the Mises-Mises theory. In the case of the Tresca-Tresca theory, however, the effect of simply supported edge was remarkable also in the distribution of these quantities.

Figs. 1.12 and 1.13, furthermore, show a comparison of the three kinds of theories in the variation of the maximum deflection and maximum stress. As observed in Fig. 1.12, just as in the numerical results of A. M. Whal for rotating disks[19], the Mises-Mises theory gives much smaller deformation than the Tresca-Mises and Tresca-Tresca theories, and therefore it gives the results of unsafe

side. This should be a general trend when the external loads are prescribed, because the Mises criterion always gives smaller (or equal) values of effective stress than that of Tresca's for every state of stress and the small difference of equivalent stress gives rise to a large discrepancy of the deformation due to the significant non-linearity of the creep law. As regards the maximum stress, however, the Mises-Mises theory gives larger values than the others (Fig. 1.13) and hence on the safer side in this respect, which is a different trend from that of Whal's[19] concerning maximum stress. Then, it is difficult to lead a straightforward conclusion as regards the suitable theory for the purpose of creep design of rather complicated structures.

It should be noticed, however, that in addition to the stress the state of deformation is also required in creep design and the difference between the predictions of deformation due to the Mises and Tresca theories is very significant because of the highly non-linear character of creep law. Hence, the more elaborate theories should be employed in creep analyses when accurate predictions of stress and deformation are required.

4.2. Circular cylindrical shells under variable internal pressure[2]

Although it is obvious that the strain- and the time-hardening hypothesis in the presence of stress variation give different results from each other, such works have been so far quite scarce as to investigate quantitatively the difference between these two hardening hypotheses when they are applied to the practical problems. In the preceding article, therefore, we illustrated the difference in the case of simply supported circular cylindrical shells with closed ends subjected to constant internal pressure on the basis of the Mises-Mises, Tresca-Mises and

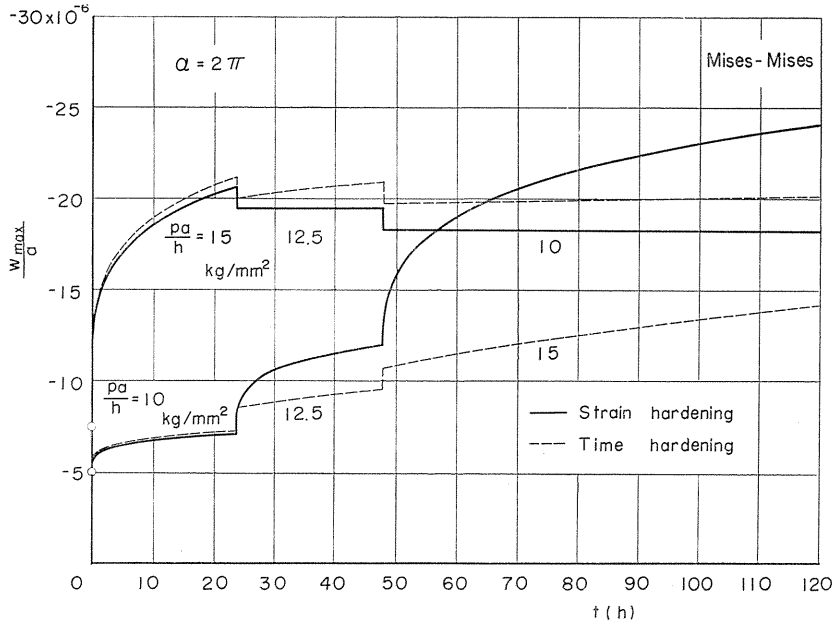

(a) step-wise increase and step-wise decreaes

FIG. 1.14. Variation of the maximum deflection in the case of variable internal pressure.

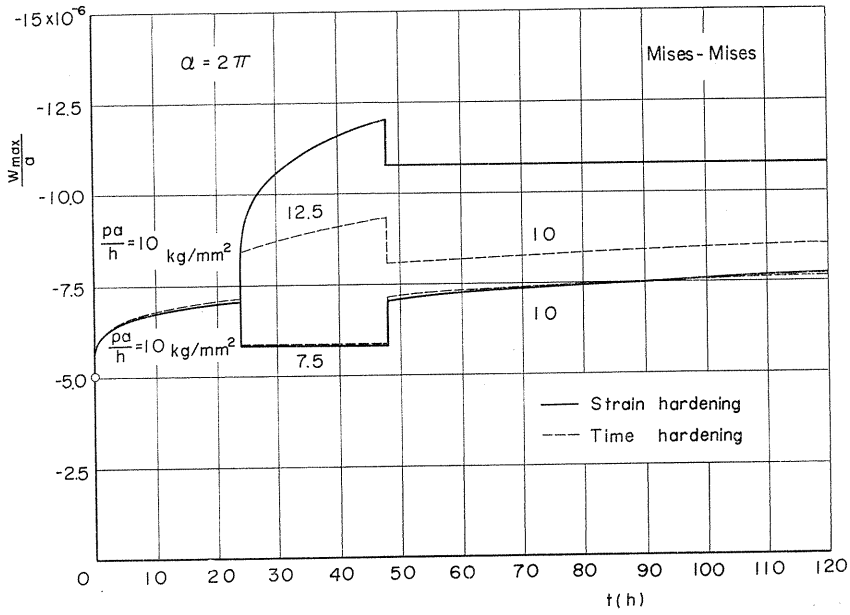

(b) temporary increase and temporary decrease

FIG. 1.14. Variation of the maximum deflection in the case of variable internal pressure.

Tresca-Tresca theories, and showed that the differences between the results due to these two kinds of hardening hypotheses resulting from re-distribution of stress during the creep are less than few per cent in every case.

In the present article, furthermore, we analyse the creep deformation of a circular cylindrical shell subjected to step-wisely varying pressure according to the Mises-Mises theory in order to investigate the difference between these hardening hypotheses in the case of varying external loads.

The results for shell of $\alpha=2\pi$, as an example, are shown in Fig. 1.14 (a) and (b), where internal pressure is changed by $pa/h=2.5$ kg/mm^2 at $t=24$ and 48 hr, respectively. It will be recognized that the difference between the results of the strain-hardening and the time-hardening theory is about 20 and 40 per cent for the pressure increase of 25 and 50 per cent in magnitude. However, in the case of pressure decrease of the same amount, the difference is less than 10 per cent. For the temporary drop of load shown in Fig. 1.14 (b), in particular, the difference between the results of both hypotheses is almost negligible. Although the difference between the two kinds of hardening hypotheses may depend upon the time and the magnitude of change of stress, of course, it can be concluded, referring to the intrinsic nature of hardening hypotheses, that in case of step-up of a certain magnitude of load the strain-hardening hypothesis always gives larger values of deformation than the other and vice versa in case of step-down of load; these differences are the larger the later is the change of load.

5. Conclusion

Transient creep analysis of shells of revolution was developed on the basis of the strain-hardening and the time-hardening hypothesis. The creep theories of Mises-Mises, Tresca-Mises and Tresca-Tresca type and the power creep law were postulated. Total strain was assumed to consist of elastic and creep components. Equations of equilibrium were replaced by the corresponding difference equations in regards to the rate of displacement, and the solution of the resulting simultaneous linear equations was integrated numerically with respect to time.

Calculations were performed for pressurised circular cylindrical shells of 0.15 per cent carbon steel at 450°C. As a first example, simply supported shells of $\alpha=\pi$ (short) and $\alpha=2\pi$ (long) with closed ends under constant internal pressure were selected. The Mises-Mises theory was found to predict the deformation which is 40 and 80 per cent smaller than the Tresca-Mises and the Tresca-Tresca theory, respectively. As regards the maximum stress, however, the Mises-Mises theory gave larger values than the other theories and is on the safer side in this respect. Then, it is difficult to lead a straightforward conclusion as regards the suitable creep theory for the design of rather complicated structures. Consequently, the modification to the elementary theory seems to have large significance in creep theory, because not only the state of stress but also the state of deformation are required in creep design and the difference between the predictions of deformation due to the Mises and the Tresca criterion is very large on account of high non-linear character of creep law.

The difference between the results due to the strain-hardening and time-hardening hypotheses was, in these shells, less than few per cent in spite of large local variation of stress. The maximum values of deflection and circumferential components of membrane force were observed at the center in the shell of $\alpha=\pi$, and in the vicinity of supported ends in the case of $\alpha=2\pi$ (except the results at $t=100$ hr due to the Tresca-Tresca theory and the strain-hardening hypothesis, where the maximum values occured at the center of shells just as in the shell of $\alpha=\pi$). They were 5 to 15 per cent larger than those of the long thin circular tube without regard to the effect of supported ends. These location of peak values are important from the viewpoint of creep design.

The simply supported shells of $\alpha=2\pi$ with closed ends subjected to variable load were analysed according to the Mises-Mises theory as the second example. Step-wise increase of internal pressure of 25 to 50 per cent in magnitude induced the difference of about 20 to 40 per cent between the results of two kinds of hardening hypotheses. In the case of pressure decrease of same magnitude, the difference was less than 10 per cent.

Part II. Steady-State Creep of Shells of Revolution[5)~9)]

1. Introduction

In the preceding Part, we analysed the transient creep of shells, and revealed the process up to the steady-state during which the creep rate decreases with the lapse of time and the elastic-plastic strain changes in accordance with the increase of creep strain. According to the numerical results for pressurised circular cylindrical shells, the variation of stress distribution in the case of constant load ends in relatively short time, and steady-state is realized actually when creep strain has increased to about 15 to 20 times as much as the elastic-plastic strain. Hence, the analysis of steady-state creep is also very important because it covers the majority of the total creep process, especially in case of relatively low stress.

Although many authors have discussed the steady-state creep of shells[26)], most of these works are concerned with some approximate analyses due to certain simplified assumptions[27)~41)]. In these analyses, accordingly, it remains open to examine the validity of the assumptions employed, and the works concerning with the shells other than the cylindrical ones are quite small[32)].

The informations of steady-state creep may be also obtained, as observed in the preceding Part, from the results of transient creep analysis as the limiting state of infinite creep strain. In such analysis, however, the stress strain-rate relation has a complicated form because the elastic-plactic strain should be also taken into account besides the creep strain. Then, it is impossible to make the relations not to include the material constant explicitly by rewriting them in terms of non-dimensional quantities. Therefore, in such problems, unlike the case of steady-state creep, one cannot obtain any general idea of the creep of shells which should be independent of the material law. The primary aim of the previously mentioned work of R. K. Penny[12)], in fact, is to establish the steady-state creep response which should appear when the creep rate has tended to constant after sufficiently long time. Accordingly, it will make a significant contribution to the engineering practice to establish accurate and direct analyses of the steady-state creep of the general shells of revolution, and derive a general conclusion which is independent of the mechanical properties of material.

In the present part, we derive at first fundamental equations of the steady-state creep of the shells of revolution by applying the extended Newton method[42)~45)] under the assumption of the creep theory of Mises type and the power creep law. In this problem, as will be observed later, integrals of the unknown variables or conversely the solution of integral equations as regards the variables appear in the governing differential equations on account of the non-linearity of the constitutive equation. Hence, it is necessary to dispose of such integral or integral equation adequately, which is a different situation from the case of physically linear problems[44)45)]. Thereafter, the creep behaviour of circular cylindrical shells and a partial spherical shell under internal pressure will be analysed as numerical examples of the fundamental equations thus derived. The creep behaviours of these shells, the effect of non-linearity of the creep law on the state of stress and deformation will be discussed in detail. The numerical results of the cylindrical shells, in particular, are compared with those due to the sandwich assumption.

2. Govering Equations

2.1. Equations for steady-state creep of shells of revolution

2.1.1. Basic relations

Consider again a thin shell of revolution as shown in Fig. 1.1. Equations of equilibrium and kinematic relations of the shell are given by the following expressions[21)~23)] just as in Part I:

$$\left.\begin{aligned}&\frac{d}{d\phi}(N_\phi r_0)-N_\theta r_1\cos\phi-\frac{1}{r_1}\frac{d}{d\phi}(M_\phi r_0)+M_\theta\cos\phi-Yr_0r_1=0\\&N_\phi r_0+N_\theta r_1\sin\phi+\frac{d}{d\phi}\left\{\frac{1}{r_1}\frac{d}{d\phi}(M_\phi r_0)-M_\theta\cos\phi\right\}-Zr_0r_1=0\end{aligned}\right\}\tag{2.1}$$

$$\left.\begin{aligned}\varepsilon_\phi&=\frac{1}{r_1}\frac{dv}{d\phi}-\frac{w}{r_1}-\frac{z}{r_1}\frac{d}{d\phi}\left(\frac{v}{r_1}+\frac{1}{r_1}\frac{dw}{d\phi}\right)\\\varepsilon_\theta&=\frac{v}{r_2}\cot\phi-\frac{w}{r_2}-\frac{z}{r_2}\cot\phi\left(\frac{v}{r_1}+\frac{1}{r_1}\frac{dw}{d\phi}\right)\end{aligned}\right\}\tag{2.2}$$

Though the steady-state creep of shells generally yields relatively large deflection, the small-deflection theory is assumed in the present analysis. It is because one of the primary aims of this Part is, as described previously, to reveal the general feature of the creep of shells in a certain extent of their deflection. The procedure to be developed here can be applied also to the case of large deflection.

The relation between stress and strain-rate of steady-state creep in the uniaxial state of stress is assumed to be expressed by the usual power law[14)~17)],

$$\dot{\varepsilon}=k\sigma^n\tag{2.3}$$

The last relation describes well the behaviour of steady-state creep of metals at elevated temperature provided the stress level is not so high. If we assume the isotropy and the incompressibility of material, the relation (2.3) is readily extended to the multiaxial state of stress according to the creep theory of Mises type[14)~16)]:

$$\dot{e}_{ij}=\frac{3}{2}k\sigma_e{}^{n-1}s_{ij},\quad \sigma_e=\left(\frac{3}{2}s_{ij}s_{ij}\right)^{1/2}\tag{2.4a}$$

According to Hoff's analogy[46)], results of analyses obtained by using the relation (2.4a) are analogous to those obtained by the aid of non-linear elastic law:

$$e_{ij}=\frac{3}{2}k\sigma_e{}^{n-1}s_{ij}\tag{2.4b}$$

The following analysis, therfore, will be carried out according to (2.4b) for the sake of convenience. The relations (2.4b) can be rewritten also in the form

$$s_{ij}=\frac{2}{3}k^{-1/n}\varepsilon_e{}^{(1-n)/n}e_{ij},\quad \varepsilon_e=\left(\frac{2}{3}e_{ij}e_{ij}\right)^{1/2}\tag{2.5}$$

The non-vanishing components of stress in the thin shells of revolution discussed here are σ_ϕ and σ_θ, and are expressed according to (2.5) as follows:

$$\left.\begin{aligned}&\sigma_\phi=\frac{4}{3}k^{-1/n}\varepsilon_e^{(1-n)/n}\left(\varepsilon_\phi+\frac{1}{2}\varepsilon_\theta\right),\quad \sigma_\theta=\frac{4}{3}k^{-1/n}\varepsilon_e^{(1-n)/n}\left(\varepsilon_\theta+\frac{1}{2}\varepsilon_\phi\right)\\&\varepsilon_e=\frac{2}{\sqrt{3}}(\varepsilon_\phi^2+\varepsilon_\phi\varepsilon_\theta+\varepsilon_\theta^2)^{1/2}\end{aligned}\right\}\tag{2.6}$$

The components of membrane force and bending moment in (2.1) are given by the relations

$$N_\phi=\int_{-h/2}^{h/2}\sigma_\phi dz,\ N_\theta=\int_{-h/2}^{h/2}\sigma_\theta dz \tag{2.7}$$

$$M_\phi=\int_{-h/2}^{h/2}\sigma_\phi z dz,\ M_\theta=\int_{-h/2}^{h/2}\sigma_\theta z dz \tag{2.8}$$

2.1.2. Application of the extended Newton method

Let's consider, at first, what kind of sectional variables should be taken as governing quantities in the present analysis. In the analyses of transient creep [1)~4) 10)~12)], the procedures analogous to the elastic case are applicable[47], because the total strain can be divided into the elastic and the creep component and the creep terms can be treated as inhomogenous terms of the differential equations. The shearing force and the rotation of section, therefore, may be chosen as the independent variables of the equations. It is difficult, however, to apply such an approach to the physically non-linear problems of steady-state creep, because therein elastic strain is not taken into account generally.

When we solve this problem as regards the sectional force, on the other hand, we must take account of the equations of compatibility at the same time. Thus, complicated integral equations have to be solved in order to express the strain components in terms of the sectional force, which is generally intractable.

If the components of displacement are chosen as the unknown variables, membrane force and bending moment are expressed as integrals of irrational functions of the displacement. When they are substituted into the equations of equilibrium, integrals of unknown variables appear in the differential equations (independent variables of the differential equations and integrating factor are different from each other). The disposal of these integrals is, however, simpler than the two cases mentioned above. In this case, furthermore, it is advantageous that we need not take account of the conditions of compatibility.

When the non-linear differential equations are solved with respect to the components of displacement by applying the extended Newton method, it is necessary to devise not to bring the integrals of unknown variables into the equations. Such a kind of difficulty does not arise in the physically linear problems. For a non-linear analytical function, to integrate it at first and then to linearize by expanding the integral in the neighbourhood of a certain approximate value is equivalent to linearize it at first and then to integrate the linearized function. Hence, as regards the expressions of membrane force and bending moment, if we linearize the expressions under integration symbol at first by expanding it in the vicinity of certain approximate values of displacement and then perform the integration, these sectional forces are expressed as linear functions of the small correction of displacement. Substitution of these expressions into the equations of equilibrium yields a system of linear differential equations in regard

to the small correction. These procedures mean precisely the application of the extended Newton method to the physically non-linear problem represented by non-linear differential equations.

The solution of the linear differential equations derived in this way now gives the value of small correction of displacement, and the previous approximate value may be improved by it. If the approximate value converges to a certain value with sufficient accuracy by repetition of the similar operation, we can obtain the accurate solution of displacement.

Now, let's express the actual values of displacement v, w as sums of the m-th approximations v^*, w^* and the small corrections $\bar{v}$, $\bar{w}$ as follows:

$$v = v^* + \bar{v}, \quad w = w^* + \bar{w} \tag{2.9}$$

If we substitute the above relations into (2.2) and (2.6) and neglect the higher order terms of $\bar{v}$ and $\bar{w}$, components of strain and stress take the forms

$$\begin{pmatrix} \varepsilon_\phi \\ \varepsilon_\theta \end{pmatrix} = \begin{pmatrix} \varepsilon_\phi^* + \dfrac{1}{r_1}\dfrac{d\bar{v}}{d\phi} - \dfrac{\bar{w}}{r_1} - \dfrac{z}{r_1}\dfrac{d}{d\phi}\left(\dfrac{\bar{v}}{r_1} + \dfrac{1}{r_1}\dfrac{d\bar{w}}{d\phi}\right) \\ \varepsilon_\theta^* + \dfrac{\bar{v}}{r_2}\cot\phi - \dfrac{\bar{w}}{r_2} - \dfrac{z}{r_2}\cot\phi\left(\dfrac{\bar{v}}{r_1} + \dfrac{1}{r_1}\dfrac{d\bar{w}}{d\phi}\right) \end{pmatrix} \tag{2.10}$$

$$\begin{pmatrix} \sigma_\phi \\ \sigma_\theta \end{pmatrix} =$$

$$\begin{pmatrix} \sigma_\phi^*\left[1 + \left\{\dfrac{1-n}{2n}\dfrac{2\varepsilon_\phi^* + \varepsilon_\theta^*}{\varepsilon_\phi^{*2} + \varepsilon_\phi^*\varepsilon_\theta^* + \varepsilon_\theta^{*2}} + \dfrac{1}{\varepsilon_\phi^* + \dfrac{1}{2}\varepsilon_\theta^*}\right\}\bar{\varepsilon}_\phi + \left\{\dfrac{1-n}{2n}\dfrac{2\varepsilon_\theta^* + \varepsilon_\phi^*}{\varepsilon_\phi^{*2} + \varepsilon_\phi^*\varepsilon_\theta^* + \varepsilon_\theta^{*2}} + \dfrac{1}{2}\dfrac{1}{\varepsilon_\phi^* + \dfrac{1}{2}\varepsilon_\theta^*}\right\}\bar{\varepsilon}_\theta\right] \\ \sigma_\theta^*\left[1 + \left\{\dfrac{1-n}{2n}\dfrac{2\varepsilon_\phi^* + \varepsilon_\theta^*}{\varepsilon_\phi^{*2} + \varepsilon_\phi^*\varepsilon_\theta^* + \varepsilon_\theta^{*2}} + \dfrac{1}{2}\dfrac{1}{\varepsilon_\theta^* + \dfrac{1}{2}\varepsilon_\phi^*}\right\}\bar{\varepsilon}_\phi + \left\{\dfrac{1-n}{2n}\dfrac{2\varepsilon_\theta^* + \varepsilon_\phi^*}{\varepsilon_\phi^{*2} + \varepsilon_\phi^*\varepsilon_\theta^* + \varepsilon_\theta^{*2}} + \dfrac{1}{\varepsilon_\theta^* + \dfrac{1}{2}\varepsilon_\phi^*}\right\}\bar{\varepsilon}_\theta\right] \end{pmatrix}$$

$$= \begin{bmatrix} \sigma_\phi^* \\ \sigma_\theta^* \end{bmatrix} + \begin{bmatrix} I_{11}^* & I_{12}^* & I_{13}^* & I_{14}^* & I_{15}^* \\ I_{21}^* & I_{22}^* & I_{23}^* & I_{24}^* & I_{25}^* \end{bmatrix} \begin{pmatrix} \bar{v} \\ d\bar{v}/d\phi \\ \bar{w} \\ d\bar{w}/d\phi \\ d^2\bar{w}/d\phi^2 \end{pmatrix} \tag{2.11}$$

where ε_ϕ^*, ε_θ^*, σ_ϕ^* and σ_θ^* denote the values which result from (2.2) and (2.6) by replacing v, w with the m-th approximations v^*, w^*. Coefficients I_{rs}^* ($r=1, 2$; $s=1, 2, \ldots, 5$) in the last relations, furthermore, have the forms

$$\left.\begin{aligned} I_{r1}^* &= -\frac{z}{r_1}\frac{d}{d\phi}\left(\frac{1}{r_1}\right)J_{r1}^* + \frac{\cot\phi}{r_2}\left(1 - \frac{z}{r_1}\right)J_{r2}^*, \quad I_{r2}^* = \frac{1}{r_1}\left(1 - \frac{z}{r_1}\right)J_{r1}^*, \quad I_{r3}^* = -\frac{1}{r_1}J_{r1}^* - \frac{1}{r_2}J_{r2}^* \\ I_{r4}^* &= -\frac{1}{r_1}\frac{d}{d\phi}\left(\frac{1}{r_1}\right)J_{r1}^* - \frac{z}{r_1}\frac{\cot\phi}{r_2}J_{r2}^*, \quad I_{r5}^* = -\frac{1}{r_1}\frac{z}{r_1}J_{r1}^*, \quad (r=1, 2) \end{aligned}\right\} \tag{2.12}$$

where J^*_{rs} $(r=1, 2\,;\ s=1, 2)$ are functions of v^*, w^* and are expressed as follows:

$$\left.\begin{aligned} J^*_{11} &= \sigma^*_\phi\left\{\frac{1-n}{2n}\frac{2\varepsilon^*_\phi+\varepsilon^*_0}{\varepsilon^{*2}_\phi+\varepsilon^*_\phi\varepsilon^*_0+\varepsilon^{*2}_0}+\frac{1}{\varepsilon^*_\phi+\frac{1}{2}\varepsilon^*_0}\right\},\quad J^*_{12} = \sigma^*_\phi\left\{\frac{1-n}{2n}\frac{2\varepsilon^*_0+\varepsilon^*_\phi}{\varepsilon^{*2}_\phi+\varepsilon^*_\phi\varepsilon^*_0+\varepsilon^{*2}_0}+\frac{1}{2}\frac{1}{\varepsilon^*_\phi+\frac{1}{2}\varepsilon^*_0}\right\}\right| \\ J^*_{21} &= \sigma^*_0\left\{\frac{1-n}{2n}\frac{2\varepsilon^*_\phi+\varepsilon^*_0}{\varepsilon^{*2}_\phi+\varepsilon^*_\phi\varepsilon^*_0+\varepsilon^{*2}_0}+\frac{1}{2}\frac{1}{\varepsilon^*_0+\frac{1}{2}\varepsilon^*_\phi}\right\},\quad J^*_{22} = \sigma^*_\phi\left\{\frac{1-n}{2n}\frac{2\varepsilon^*_0+\varepsilon^*_\phi}{\varepsilon^{*2}_\phi+\varepsilon^*_\phi\varepsilon^*_0+\varepsilon^{*2}_0}+\frac{1}{\varepsilon^*_0+\frac{1}{2}\varepsilon^*_\phi}\right\}\right| \end{aligned} \tag{2.13}$$

When the relations (2.11) are substituted into (2.7) and (2.8), the components of membrane force and bending moment are expressed as linear functions of $\bar{v}$ and $\bar{w}$, and have the forms

$$\begin{pmatrix} N_\phi \\ N_0 \\ M_\phi \\ M_0 \end{pmatrix} = \begin{pmatrix} N^*_\phi \\ N^*_0 \\ M^*_\phi \\ M^*_0 \end{pmatrix} + \begin{pmatrix} K^*_{11}K^*_{12}\cdots K^*_{15} \\ K^*_{21}K^*_{22}\cdots K^*_{25} \\ L^*_{11}L^*_{12}\cdots L^*_{15} \\ L^*_{21}L^*_{22}\cdots L^*_{25} \end{pmatrix} \begin{pmatrix} \bar{v} \\ d\bar{v}/d\phi \\ \bar{w} \\ d\bar{w}/d\phi \\ d^2\bar{w}/d\phi^2 \end{pmatrix} \tag{2.14}$$

where

$$N^*_\phi = \int_{-h/2}^{h/2}\sigma^*_\phi dz,\quad N^*_0 = \int_{-h/2}^{h/2}\sigma^*_0 dz \tag{2.15a}$$

$$M^*_\phi = \int_{-h/2}^{h/2}\sigma^*_\phi z dz,\quad M^*_0 = \int_{-h/2}^{h/2}\sigma^*_0 z dz \tag{2.15b}$$

$$K^*_{rs} = \int_{-h/2}^{h/2} I^*_{rs} dz,\quad L^*_{rs} = \int_{-h/2}^{h/2} I^*_{rs} z dz \tag{2.16}$$

Finally, the substitution of (2.14) into (2.1) provides the following simultaneous differential equations with respect to $\bar{v}$ and $\bar{w}$:

$$\left.\begin{aligned} &\frac{d}{d\phi}\left\{r_0\left(K^*_{11}\bar{v}+K^*_{12}\frac{d\bar{v}}{d\phi}+K^*_{13}\bar{w}+K^*_{14}\frac{d\bar{w}}{d\phi}+K^*_{15}\frac{d^2\bar{w}}{d\phi^2}\right)\right\}-\frac{1}{r_1}\frac{d}{d\phi}\left\{r_0\left(L^*_{11}\bar{v}+L^*_{12}\frac{d\bar{v}}{d\phi}\right.\right. \\ &\quad\left.\left.+L^*_{13}\bar{w}+L^*_{14}\frac{d\bar{w}}{d\phi}+L^*_{15}\frac{d^2\bar{w}}{d\phi^2}\right)\right\}+\cos\phi\left\{(L^*_{21}-r_1K^*_{21})\bar{v}+(L^*_{22}-r_1K^*_{22})\frac{d\bar{v}}{d\phi}\right. \\ &\quad\left.+(L^*_{23}-r_1K^*_{23})\bar{w}+(L^*_{24}-r_1K^*_{24})\frac{d\bar{w}}{d\phi}+(L^*_{25}-r_1K^*_{25})\frac{d^2\bar{w}}{d\phi^2}\right\} \\ &\quad = Yr_0r_1-\frac{d}{d\phi}(N^*_\phi r_0)+\frac{1}{r_1}\frac{d}{d\phi}(M^*_\phi r_0)-\cos\phi(M^*_0-N^*_0r_1) \\ &\left(\frac{r_0}{r_1}K^*_{11}+K^*_{21}\sin\phi\right)\bar{v}+\left(\frac{r_0}{r_1}K^*_{12}+K^*_{22}\sin\phi\right)\frac{d\bar{v}}{d\phi}+\left(\frac{r_0}{r_1}K^*_{13}+K^*_{23}\sin\phi\right)\bar{w} \\ &\quad+\left(\frac{r_0}{r_1}K^*_{14}+K^*_{24}\sin\phi\right)\frac{d\bar{w}}{d\phi}+\left(\frac{r_0}{r_1}K^*_{15}+K^*_{25}\sin\phi\right)\frac{d^2\bar{w}}{d\phi^2}+\frac{1}{r_1}\frac{d}{d\phi}\left[\frac{1}{r_1}\frac{d}{d\phi}\right. \end{aligned}\right| \tag{2.17}$$

$$\left\{ r_0\left(L_{11}^*\bar{v}+L_{12}^*\frac{d\bar{v}}{d\phi}+L_{13}^*\bar{w}+L_{14}^*\frac{d\bar{w}}{d\phi}+L_{15}^*\frac{d^2\bar{w}}{d\phi_2}\right)\right\}$$
$$+\cos\phi\left\{L_{21}^*\bar{v}+L_{22}^*\frac{d\bar{v}}{d\phi}+L_{23}^*\bar{w}+L_{24}^*\frac{d\bar{w}}{d\phi}+L_{25}^*\frac{d^2\bar{w}}{d\phi^2}\right\}\Big]$$
$$=Zr_0-\left(\frac{r_0}{r_1}N_\phi^*+N_\theta^*\sin\phi\right)-\frac{1}{r_1}\frac{d}{d\phi}\left\{\frac{1}{r_1}\frac{d}{d\phi}(M_\phi^* r_0)-M_\theta^*\cos\phi\right\}$$

The boundary conditions of the above equations are, for example,

Center : $$\phi=0,\ \bar{v}=\frac{d^2\bar{v}}{d\phi^2}=\frac{d\bar{w}}{d\phi}=0 \tag{2.18a}$$

Clamped edge: $$\phi=\beta,\ \bar{v}=\bar{w}=\frac{d\bar{w}}{d\phi}=0 \tag{2.18b}$$

Simply supported edge: $$\phi=\beta,\ \bar{v}=\bar{w}=\bar{M}_\phi=0 \tag{2.18c}$$

In order to obtain the solution corresponding to a certain value of n, it is necessary to calculate the values of v and $\bar{w}$ repeatedly until v^* and w^* converge sufficiently to certain values. Then, the equation (2.17) must be solved at every time of the repetition.

If the derivatives with respect to ϕ are replaced by the centered difference[24], the equations (2.17) together with (2.18) are reduced to the following simultaneous linear equations with respect to $\bar{v}_i$ and $\bar{w}_i$:

$$\boldsymbol{A}X=\boldsymbol{B} \tag{2.19}$$

The expressions of $\boldsymbol{A}$, X and $\boldsymbol{B}$ will be given by specifying the geometry of the shell.

Once the values of $\bar{v}_i$ and $\bar{w}_i$ have been determined from the above procedure, the components of strain, stress, membrane force and bending moment at each mesh point can be immediately calculated by the finite-difference relations corresponding to (2.2), (2.6), (2.7) and (2.8).

2.2. Governing equations for pressurised circular cylindrical shells[5)~8)]

The governing equations for circular cylindrical shells under internal pressure can be again obtained by the replacements

$$\left.\begin{aligned}&\phi=\frac{\pi}{2},\ r_0=r_2=a,\ r_1d\phi=dx,\ r_1=\infty\\&Y=0,\ Z=-p\end{aligned}\right\} \tag{2.20}$$

The discussion concerning the equations for the relevant shells was already reported in detail[5)~8)], and will be omitted here.

If the shell is sufficiently long, in particular, the central part of the shell is free from the influence of the end conditions. Then, a simple closed form solution may be obtained for this portion, and can be expressed as follows:

$$\left.\begin{aligned}&\frac{w}{ak\left(\frac{pa}{h}\right)^n}=-1,\quad \frac{u}{lk\left(\frac{pa}{h}\right)^n}=-\frac{1}{2}\frac{x}{l}\\&\frac{M_x}{pah}=\frac{M_\theta}{pah}=0,\quad \frac{N_x}{pa}=0,\quad \frac{N_\theta}{pa}=1\end{aligned}\right\}\quad\text{(open end)} \tag{2.21a}$$

$$\left.\begin{aligned} &\frac{w}{ak\left(\frac{pa}{h}\right)^n}=-\left(\frac{\sqrt{3}}{2}\right)^{n+1}, \quad \frac{u}{lk\left(\frac{pa}{h}\right)^n}=0 \\ &\frac{M_x}{pah}=\frac{M_\theta}{pah}=0, \quad \frac{N_x}{pa}=\frac{1}{2}, \quad \frac{N_\theta}{pa}=1 \end{aligned}\right\} \quad \text{(closed end)} \qquad (2.21\,\text{b})$$

2.3. Governing equations for pressurised spherical shells[9]

The basic relations for this problem can be directly obtained by applying the replacements

$$r_1=r_2=a, \quad r_0=a\sin\phi, \quad Y=0, \quad Z=-p \qquad (2.22)$$

to the preceding relations for general shells of revolution.

If the previously defined non-dimensional quantities are introduced together with (2.22), the relations (2.1), (2.18), (2.2), (2.6), (2.7) and (2.8) turn out to the following forms:

$$\left.\begin{aligned} &\frac{d}{d\phi}\{(n_\phi-Hm_\phi)\sin\phi\}-(n_\theta-Hm_\theta)\cos\phi=0 \\ &\frac{d^2}{d\phi^2}(n_\phi\sin\phi)-\frac{d}{d\phi}(n_\theta\cos\phi)+(n_\phi+n_\theta-2)\sin\phi=0 \end{aligned}\right\} \qquad (2.23)$$

$$\left.\begin{aligned} &\phi=0, \quad V=\frac{d^2V}{d\phi^2}=\frac{dW}{d\phi}=0 \qquad \text{(center)} \\ &\phi=\beta, \quad V=W=\frac{dW}{d\phi}=0 \qquad \text{(clamped edge)} \\ &\phi=\beta, \quad V=W=m_\phi=0 \qquad \text{(simply supported edge)} \end{aligned}\right\} \qquad (2.24)$$

$$\left.\begin{aligned} &E_\phi=\left(\frac{dV}{d\phi}-W\right)-\frac{1}{2}H\eta\frac{d}{d\phi}\left(V+\frac{dW}{d\phi}\right), \\ &E_\theta=(V\cot\phi-W)-\frac{1}{2}H\eta\cot\phi\left(V+\frac{dW}{d\phi}\right) \end{aligned}\right\} \qquad (2.25)$$

$$\left.\begin{aligned} &S_\phi=\frac{4}{3}\left(\frac{1}{2}\right)^{1/n}E_e^{(1-n)/n}\left(E_\phi+\frac{1}{2}E_\theta\right), \quad S_\theta=\frac{4}{3}\left(\frac{1}{2}\right)^{1/n}E_e^{(1-n)/n}\left(E_\theta+\frac{1}{2}E_\phi\right) \\ &E_e=\frac{2}{\sqrt{3}}(E_\phi^2+E_\phi E_\theta+E_\theta^2)^{1/2} \end{aligned}\right\} \qquad (2.26)$$

$$n_\phi=\frac{1}{2}\int_{-1}^{1}S_\phi d\eta, \quad n_\theta=\frac{1}{2}\int_{-1}^{1}S_\theta d\eta \qquad (2.27)$$

$$m_\phi=\frac{1}{4}\int_{-1}^{1}S_\phi\eta d\eta, \quad m_\theta=\frac{1}{4}\int_{-1}^{1}S_\theta\eta d\eta \qquad (2.28)$$

If we assume again that the actual values of the reduced displacement V, W consist of the m-th approximations V^*, W^* and the small corrections to them $\overline{V}$, $\overline{W}$ and proceed analogously as before, we obtain directly the governing equations for spherical shells under internal pressure.

In the case of a complete shell, in particular, solutions of closed form may be easily obtained. The components of displacement, membrane force and bending moment are given by the following relations[15]:

$$\left.\begin{aligned} &\frac{w}{\frac{ka}{2}\left(\frac{pa}{2h}\right)^n}=-1,\quad \frac{v}{\frac{ka}{2}\left(\frac{pa}{2h}\right)^n}=0,\quad \frac{N_\phi}{\left(\frac{pa}{2}\right)}=\frac{N_\theta}{\left(\frac{pa}{2}\right)}=1\\ &\frac{M_\phi}{\left(\frac{pah}{2}\right)}=\frac{M_\theta}{\left(\frac{pah}{2}\right)}=0 \end{aligned}\right\} \tag{2.29}$$

3. Method of Calculation

In order to start the preceding calculation, certain approximate values of the components of displacement must be specified. Expressions (2.11) may be rewritten as follows:

$$\begin{pmatrix}\sigma_\phi\\ \sigma_\theta\end{pmatrix}=\begin{pmatrix}\sigma_\phi^*\\ \sigma_\theta^*\end{pmatrix}+\begin{pmatrix}\dfrac{1-n}{2n}\dfrac{(2\varepsilon_\phi^*+\varepsilon_\theta^*)\bar{\varepsilon}_\phi+(2\varepsilon_\theta^*+\varepsilon_\phi^*)\bar{\varepsilon}_\theta}{\varepsilon_\phi^{*2}+\varepsilon_\phi^*\varepsilon_\theta^*+\varepsilon_\theta^{*2}}\sigma_\phi^*+\dfrac{4}{3}k^{-1/n}(\varepsilon_e^*)^{(1-n)/n}\left(\bar{\varepsilon}_\phi+\dfrac{1}{2}\bar{\varepsilon}_\theta\right)\\ \dfrac{1-n}{2n}\dfrac{(2\varepsilon_\phi^*+\varepsilon_\theta^*)\bar{\varepsilon}_\phi+(2\varepsilon_\theta^*+\varepsilon_\phi^*)\bar{\varepsilon}_\theta}{\varepsilon_\phi^{*2}+\varepsilon_\phi^*\varepsilon_\theta^*+\varepsilon_\theta^{*2}}\sigma_\theta^*+\dfrac{4}{3}k^{-1/n}(\varepsilon_e^*)^{(1-n)/n}\left(\bar{\varepsilon}_\theta+\dfrac{1}{2}\bar{\varepsilon}_\phi\right)\end{pmatrix} \tag{2.30}$$

By the replacements

$$n=1,\quad (\quad)^*\to 0,\quad (\bar{\ })\to(\quad) \tag{2.31}$$

the relations (2.30) become

$$\sigma_\phi=\frac{4}{3}k^{-1}\left(\varepsilon_\phi+\frac{1}{2}\varepsilon_\theta\right),\quad \sigma_\theta=\frac{4}{3}k^{-1}\left(\varepsilon_\theta+\frac{1}{2}\varepsilon_\phi\right) \tag{2.32}$$

which coincide with the relations (2.6) in the case of $n=1$. The expression (2.11), therefore, gives the exact relations for $n=1$. Thus, the governing equations (2.17) which result from (2.11), (2.7), (2.8) and (2.1) are exact ones in the case of $n=1$. In other words, the equation (2.19) together with the replacements (2.31) readily furnishes the solution for the linear case, and hence it may be used as the first approximation to the solution of $n=1+\Delta n$.

If the solution for $n=n_0$ has been obtained, it can be used as the first approximation v_i^*, w_i^* to the solution for $n=n_0+\Delta n$. The matrix $\boldsymbol{A}$ and vector $\boldsymbol{B}$ of (2.19) can be determined by calculating K_{rs}^*, L_{rs}^* from (2.12), (2.13) and (2.16). The second approximations of v_i, w_i for $n=n_0+\Delta n$ will be furnished with solutions of $\bar{v}_i$, $\bar{w}_i$ of (2.19) in the next expressions

$$v_i=v_i^*+\lambda\bar{v}_i,\quad w_i=w_i^*+\lambda\bar{w}_i \tag{2.33}$$

where λ $(0<\lambda\leqq 1)$ is a relaxation parameter introduced to avoid the divergence of the iterative solution. By solving (2.19) again after calculating $\boldsymbol{A}$ and $\boldsymbol{B}$ from the second approximation, the third approximation can be determined from (2.33). When the condition

$$\mathrm{Max}\left\{\frac{\bar{v}_i}{v_i},\ \frac{\bar{w}_i}{w_i};\ i=0,\ 1,\ \ldots,\ N\right\}\leqq\delta \tag{2.34}$$

is satisfied after iterating the similar procedures for proper small value δ, the values of v_i and w_i may attain to an accurate solution for $n=n_0+\Delta n$. The components of strain, stress, membrane force and beding moment are calculated by (2.2), (2.6), (2.7) and (2.8) with the use of these values.

The solution for arbitrary values of n will be determined by increasing n step by step and applying the similar procedure.

4. Results of Calculation and Discussion

4.1. Simply supported circular cylindrical shells under internal pressure[5)6)9)]

The creep behaviour of a simply supported circular cylindrical shell of $\alpha=2\pi$ with open ends is discussed first. The meaning of the parameter α is the same as in Part I.

In the present example, the values $\lambda=1$ and $\delta=10^{-7}$ were assumed in (2.33) and (2.34) together with $\Delta n=1$. The condition (2.34) was satisfied by the few iterations for every value of n.

Procedures described above were programmed according to FORTRAN IV, and calculations were all carried out in double precision (13 digits) by using digital computer HITAC-5020. The programme consists of about 68,000 machine words in case of $g=1/50$. The time of calculation was, for example, about 120 sec for the shell of $\alpha=2\pi$ and $n=1$ through 5.

As already pointed out, the replacement of differential equation (2.17) with the corresponding difference equation (2.19) involves truncation errors of the order of g^2 ($g=1/2N$, N; number of division over the half length of shell). Therefore, the calculations were carried out with $g=1/25$ and $1/50$ in order to examine the magnitude of the error. The numerical results due to two kinds of g together with the analytical results[21)] are shown in Table 2.1 for linear case $n=1$. It should be noticed that the difference between the results for $g=1/25$ and $1/50$ are less than 1 per cent, and that between the analytical and the numerical result with $g=1/50$ is less than 0.5 per cent. Since the discrepancy between the results of $g=1/25$ and $1/50$ in the case of $n=3$ and 5 has been ascertained to be almost the same magnitude as in $n=1$, the results according to $g=1/50$ may be certified to be accurate enough for practical purposes. The following results, therefore, have been obtained by using the difference interval $g=1/50$ throughout. In the following, the numerical results for each value of creep exponent n are shown in Figs. 2.1 through 2.4.

Fig. 2.1 shows the distribution of deflection, where the ordinate represents the non-dimensional values reduced by the corresponding deflection (2.21 a) of long thin circular tube without end effect. The maximum values of $w/ak(pa/h)^n$ for $n=1$, 3 and 5 are -1.06, -1.09 and -1.10, which are larger by 6~10 per cent than those of the long tube. Since the values of deflection at center are -0.996 ($n=1$), -0.997 ($n=3$) and -1.010 ($n=5$), the influence of supported end on the deflection is very small in this part.

Although the membrane force N_θ/pa shown in Fig. 2.2 takes almost the same values in the central part of the shell as those of long thin circular tube, the maximum values are about 6 ($n=1$) ~2 ($n=5$) per cent larger than that of the long tube.

The bending moment in the axial direction (Fig. 2.3), on the other hand, is almost 0 in the range $2x/l<0.4$, while it shows significant values in the range

TABLE 2.1. Comparison between the numerical results for $n=1$ and the corresponding analytical results (simply supported shell of $\alpha=2\pi$)

	$2x/l$	0	0.2	0.4	0.6	0.8	1.0
$\frac{w}{ak\left(\frac{pa}{h}\right)^n}$	Numerical ($g=1/25$)	−0.996	−0.998	−1.019	−1.064	−0.911	0
	Numerical ($g=1/50$)	−0.996	−0.998	−1.019	−1.065	−0.912	0
	Analytical [21]	−0.996	−0.998	−1.019	−1.066	−0.912	0
$\frac{M_x}{pah}$		$\times10^{-5}$	$\times10^{-2}$	$\times10^{-2}$	$\times10^{-2}$	$\times10^{-2}$	
	Numerical ($g=1/25$)	4	0.188	0.428	−1.595	−8.944	0
	Numerical ($g=1/50$)	1	0.190	0.443	−1.588	−9.003	0
	Analytical [21]	0	0.191	0.445	−1.586	−9.022	0

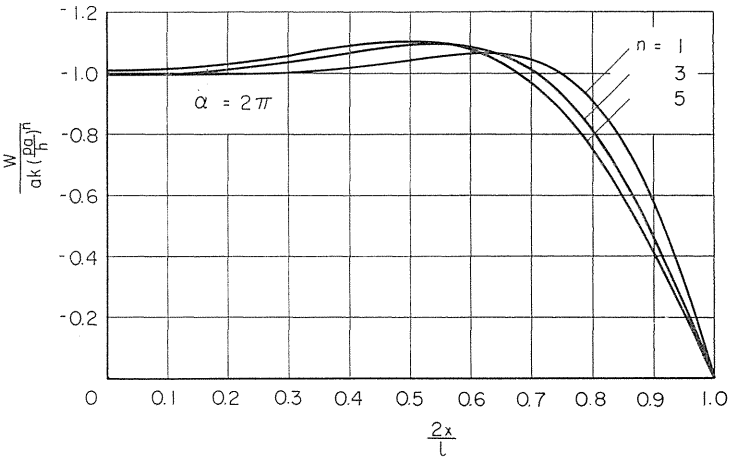

FIG. 2.1. Distribution of the displacement.

$0.6<2x/l$. It will be noticed that the distribution of M_x/pah as well as N_θ/pa becomes more uniform remarkably in the axial direction as n increases.

In Fig. 2.4, some of the present results are compared with the corresponding results obtained by Yu. N. Rabotnov on the basis of sandwich shell assumption[35)36)]. Concerning the correlation between two kinds of shell, the behaviour of both shells is assumed to coincide with each other only in the membrane state and the state of pure bending[35)]. The results of Rabotnov were calculated for a simply supported semi-infinite sandwich shell with open ends by means of the variational method.

Though the results for sandwich shell should coincide with those of homogeneous shell in case of $n=1$, the disagreement of about 0.5 per cent is observed between the solid and the dashed line in Fig. 2.4, which may be attributed to the errors of the present calculation shown in Table 1.1, and those according to the approximate relations assumed in References [35, 36].

In the cases of $n=3$ and $n=5$, on the other hand, discrepancies of about 3 ($n=3$), 4 ($n=5$) and 7 ($n=3$), 10 ($n=5$) per cent are observed for the deflection and the bending moment, respectively. These differences, however, should be referred to the errors of Rabotnov's analysis, that is, the error due to the assumption of

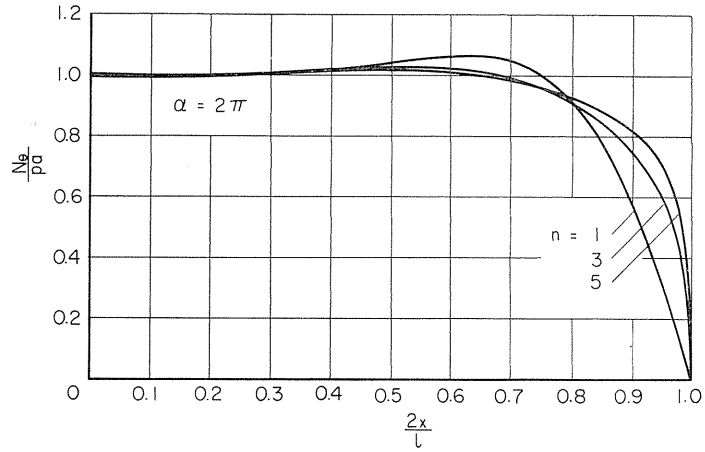

FIG. 2.2. The circumferential component of the membrane force.

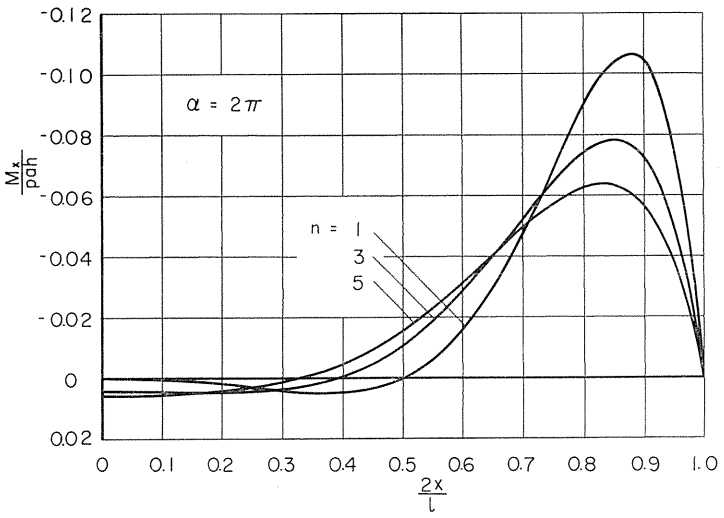

FIG. 2.3. The axial component of the bending moment.

sandwich shell and that accompanied with the variational procedure, and the errors of the present calculation described above as well as that due to the difference in the geometry of these shells. The magnitude of individual errors, however, is not clear. The errors involved in the assumptions of sandwich construction, above all, is very interesting because a number of previous works on plastic and creep analyses employed such a simplification.

In References [5] and [6], the similar results for the shell of $\alpha=\pi$ were also reported.

4.2. Clamped circular cylindrical shells under internal pressure[7][8]

The analogous results for clamped circular cylindrical shell with open ends are shown in Table 2.2 and Figs. 2.5 through 2.8.

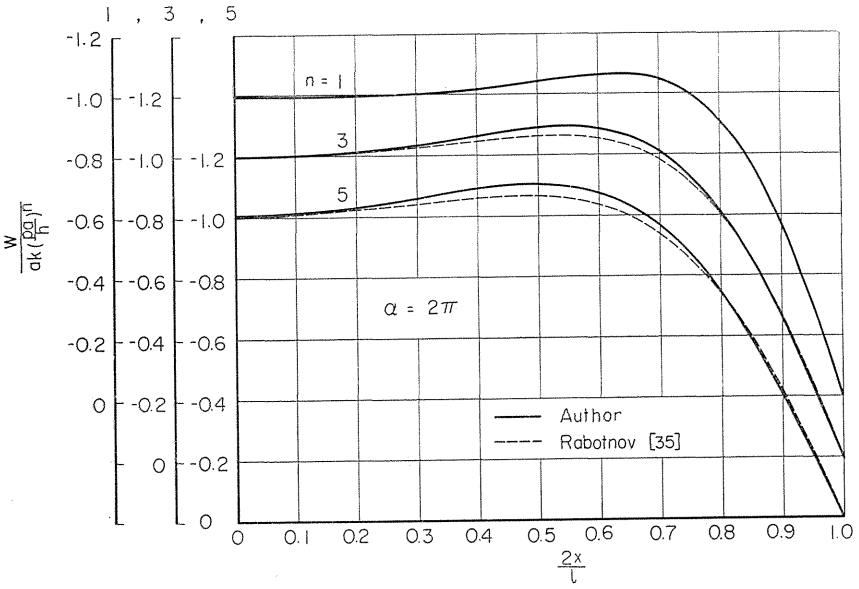

(a) deflection

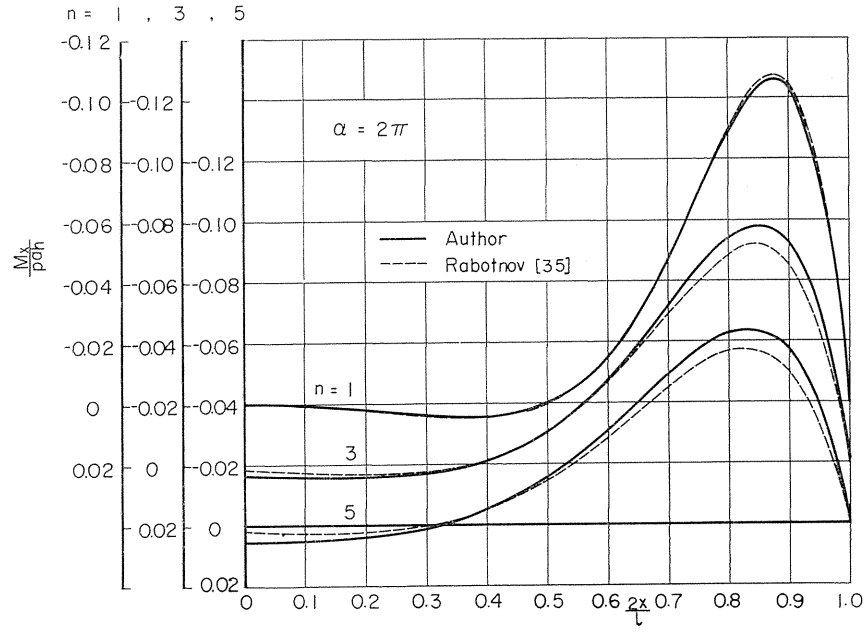

(b) bending moment

FIG. 2.4. Comparison between the present results and those for sandwich shell.

At first, the maximum values of non-dimensional deflection shown in Fig. 2.5 are -1.040 ($n=1$), -1.045 ($n=3$), -1.050 ($n=5$), respectively, and are smaller than the corresponding values for simply supported shell (Fig. 2.1) by 2 ($n=1$) $\sim$ 5 ($n=5$) per cent. Since the values of the deflections at the center, on the other hand, are -0.997 ($n=1$), -1.016 ($n=3$), -1.042 ($n=5$), a considerable effect of clamped end is observed at the center in the case of $n=3$ and 5, which is a different feature from that of Fig. 2.1. It should be noticed, therefore, that the effect of end condition prevails wider range in this case than in the supported shell.

The maximum values of membrane force shown in Fig. 2.6 are 1.043, 1.015, 1.010 for $n=1$, 3, 5 respectively, which are smaller than those of simply supported shell by about 2 ($n=1$) $\sim$ 1 ($n=5$) per cent. As observed in Fig. 2.6 and 2.7, the values of membrane force and bending moment at the center almost coincide with those of long thin circular tube (2.21 a), unlike the case of preceding deflection.

Fig. 2.8 shows the comparison between the present results and those for the clamped sandwich cylindrical shell of $\alpha=2\pi$ due to F. A. Cozzarelli *et al.*[40] which are entered with dashed lines in the figure. The correlation between the uniform and the sandwich shell is again achieved according to Rabotnov[35)36)] by requiring

TABLE 2.2. Comparion between the numerical results for $n=1$ and the corresponding analytical results (clamped shell of $\alpha=2\pi$)

	$2x/l$	0	0.2	0.4	0.6	0.8	1.0
$\frac{w}{ak\left(\frac{pa}{h}\right)^n}$	Numerical ($g=1/25$)	-0.997	-1.003	-1.031	-1.018	-0.651	0
	Numerical ($g=1/50$)	-0.996	-1.004	-1.032	-1.018	-0.644	0
	Analytical [21]	-0.996	-1.004	-1.032	-1.018	-0.641	0
$\frac{M_x}{pah}$	Numerical ($g=1/25$)	0.0012	0.0025	-0.0018	-0.0369	-0.0606	0.3230
	Numerical ($g=1/50$)	0.0013	0.0026	-0.0018	-0.0375	-0.0608	0.3308
	Analytical [21]	0.0013	0.0026	-0.0018	-0.0377	-0.0609	0.3333

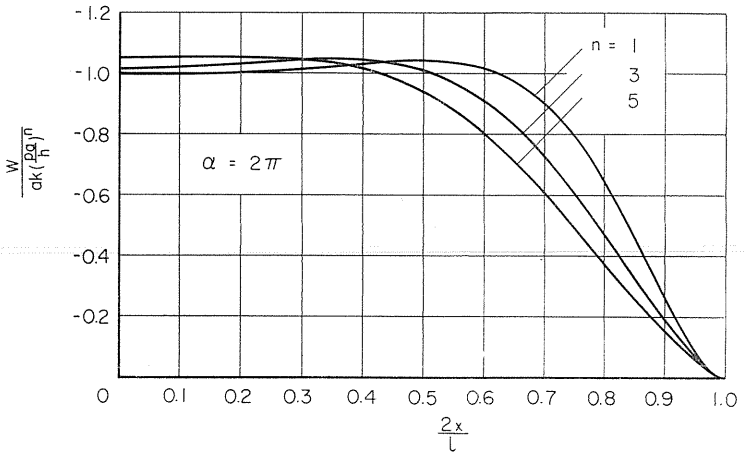

FIG. 2.5. Distribution of the deflection,

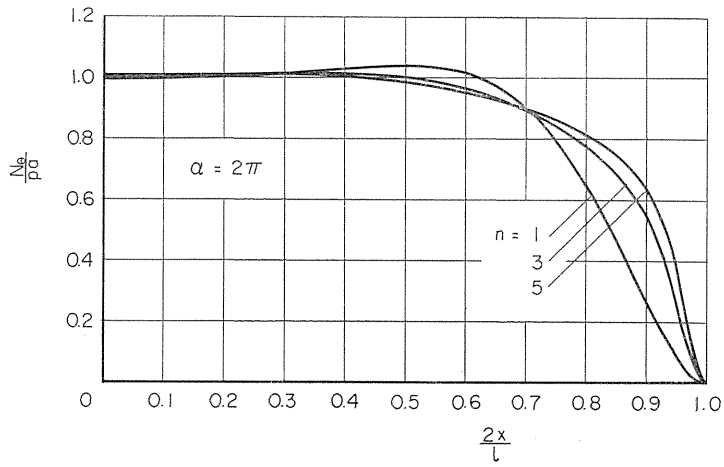

FIG. 2.6. The circumferential component of the membrane force.

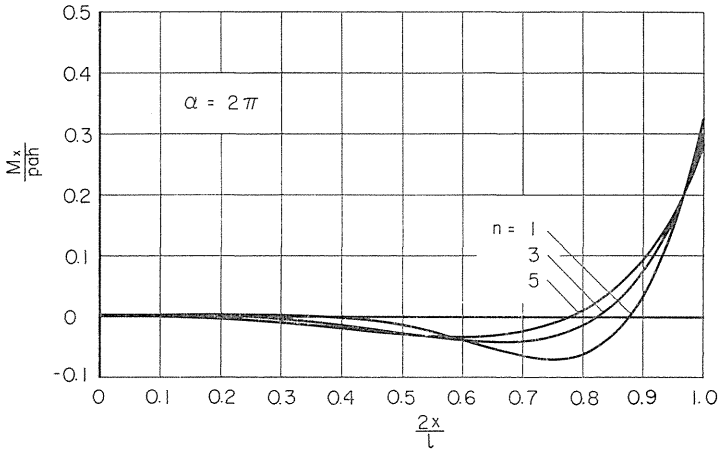

FIG. 2.7. The axial component of the bending moment.

that the behaviour of the both shells coincide with each other only in the membrane state and the state of pure bending.

Although the solution of sandwich shell should coincide exactly with that of uniform shell in case of $n=1$, the disagreement of about 0.5 per cent is observed in Fig. 2.8 (a), which may be attributed to the errors of the reproduction of dashed lines from Reference [40] in addition to that of the present calculation as already shown in Table 2.2. In the case of $n=3$ and $n=5$, the discrepancies of deflection of about 3 ($n=3$) and 5 ($n=5$) per cent are recognized in the range $0.5<2x/l<0.95$. Similar features are observed in Fig. 2.8 (b). The difference in maximum values of M_x/pah between these two kinds of results is about 1 ($n=1$), 3 ($n=3$), 10 ($n=5$) per cent, respectively.

Though the discrepancy between the full and dashed lines in these figures is small in the central portion and in the close vicinity of clamped end where the

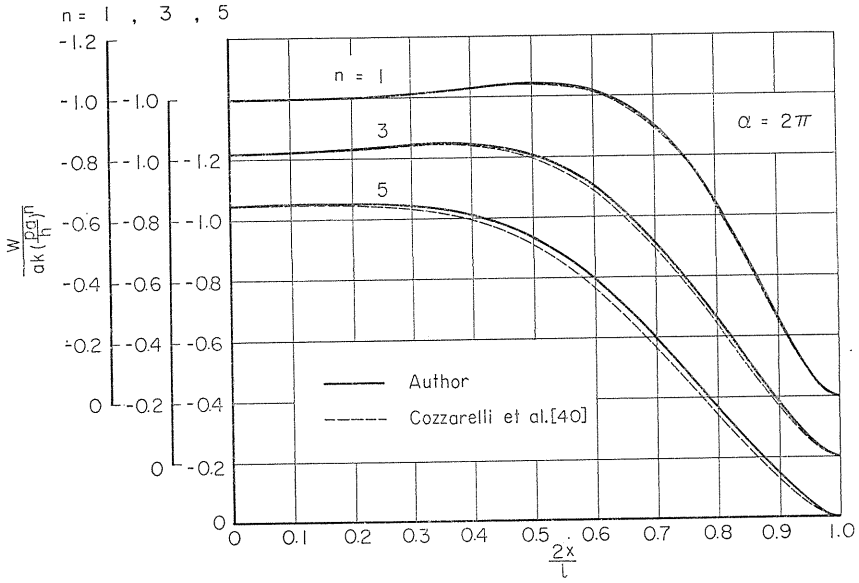

(a) deflection

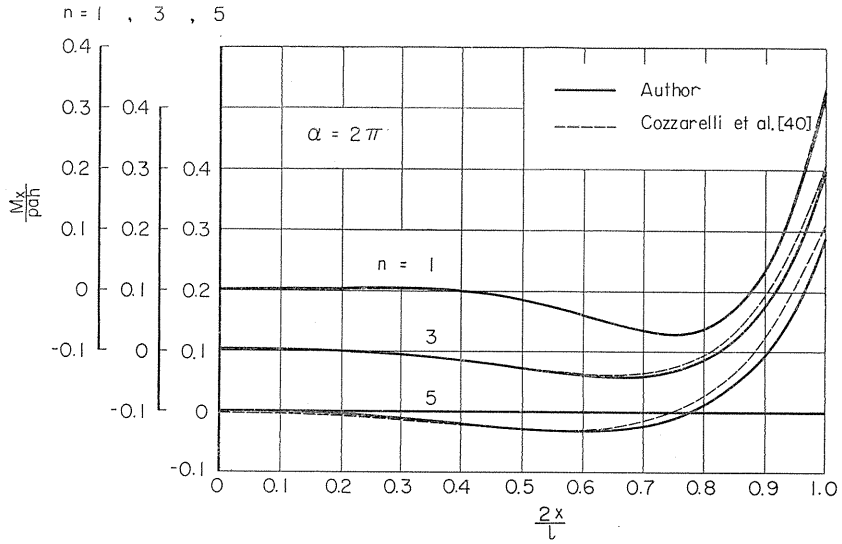

(b) bending moment

FIG. 2.8. Comparison between the present results and those for sandwich shell.

membrane force (central portion) and the bending moment (near the clamped end) predominate separately over the other, it is considerably significant in the range $0.85<2x/l<0.95$ where the effect of M_x/pah and N_θ/pa is comparable. Then, it should be noticed that this feature stems from the aforementioned assumption that the behaviour of sandwich model coincide with that of the real shell only

in the membrane state or in the state of pure bending in the case of $n \neq 1$. The sandwich model employed by Cozzarelli *et al.*, therefore, may give a close qualitative and quantitative assessment of the creep deformation of cylindrical shells of the present condition. However, in the case where the state of stress is far from the membrane state or the pure bending state, such as in a cylindrical shell which is short enough or is subject to the combined action of axial force and internal pressure, or such as in the shallow spherical shell where the effeets of bending moment are as significant as that of membrane force, the assumption of a sandwich shell may not always be a good approximation to the real shell of uniform wall thickness, especially for large value of the creep exponent. The validity of the creep analysis based on the sandwich construction in such case is open to further investigation.

In Reference [7] and [8], the analogous discussion for the shell of $\alpha = \pi$ was also presented.

4.3. Clamped spherical shells under internal pressure[9]

The numerical results for a clamped spherical shell of semi-angle $\beta = 60°$ and thickness-to-radius ration $h/a = 1/20$ are shown in Figs. 2.9 through 2.11 as well as Table 2.3.

In the present example, the values of λ and δ in (2.33) and (2.34) were assumed to be $\lambda = 1$, $\delta = 10^{-6}$. For the value $\Delta n = 0.5$, about ten times of iteration were necessary until the condition (2.33) was satisfied.

TABLE 2.3. Comparison between the numerical results for $n=1$ and the corresponding analytical results (clamped spherical shell of $\beta = 60°$, $h/a = 1/20$)

	ϕ/β	0	0.2	0.4	0.6	0.8	1.0
$\frac{w}{\frac{ka}{2}\left(\frac{pa}{2h}\right)^n}$	Numerical ($g=1/50$)	-1.348	-1.367	-1.394	-1.287	-0.719	0
	Analytical [21]	-1.361	-1.376	-1.400	-1.287	-0.712	0
$\frac{M_\phi}{\left(\frac{pah}{2}\right)}$	Numerical ($g=1/50$)	$\times 10^{-2}$ 0.651	$\times 10^{-2}$ 0.341	$\times 10^{-2}$ -0.537	$\times 10^{-1}$ -0.322	$\times 10^{-1}$ -0.334	0.190
	Analytical [21]	0.452	0.359	-0.565	-0.324	-0.324	0.189

The difference interval was assumed to be $g = \beta/50$. Table 2.3 facilitates the comparison of the present results for $n=1$ with the analytical ones for the corresponding linear elastic shell with Poisson's ration $\nu = 1/2$, as a measure to estimate the errors due to the finite-difference approximation. The analytical solutions were calculated according to Meissner's solution in the form of series[21]. It will be observed that the present results differ from the analytical ones by about 1 per cent of their maximum values. Thus, the accuracy of the present results is a little worse than that for the cylindrical shells discussed above, which may be partly ascribed to the reduction of accuracy of finite-difference approximation due to the indeterminate character of the relations at the center of shell.

Fig. 2.9, to begin with, shows the distribution of deflection, where the ordinate represents the values reduced by the values (2.29) for a complete spherical shell. It will be observed that the deflection of the present shell is larger than that of

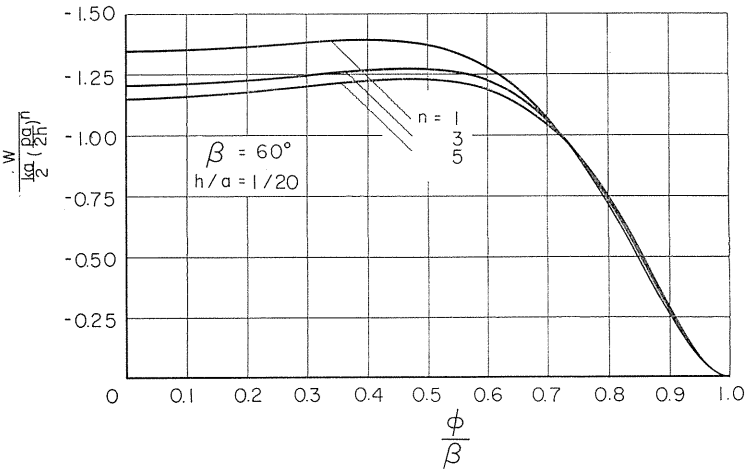

FIG. 2.9. Distribution of the deflection.

the complete shell by about 40 per cent in the case of $n=1$, and 25 per cent as well for $n=5$ which is a typical value of n for steel at elevated temperature. Thus, the rate of deformation in the partial spherical shell discussed here are subject to much more significant effect of clamped end than in the case of the preceding cylindrical shell. The effect of clamped end on the deformation of the shell is, of course, depends on the magnitude of h/a[23].

$N_\theta/(pa/2)$, as shown in Fig. 2.10, increases a little from the values about 1 at the center, takes its maximum values 1.03 ($n=1$), 1.02 ($n=3$) and 1.01 ($n=5$) at $\phi/\beta=0.4\sim0.6$, and decrease monotonously to the values about 0.5 at the clamped edge. $N_\phi/(pa/2)$, which is omitted here, takes the values nearly 1 over the whole shell. It is related to $N_\theta/(pa/2)$ by the relation $N_\phi/(pa/2)=N_\theta(pa/2)$ at the center according to the isotropy of stress and strain, and $N_\phi/(pa/2)=2N_\theta/(pa/2)$ at clamped edge on account of the relation $\varepsilon_\theta=0$.

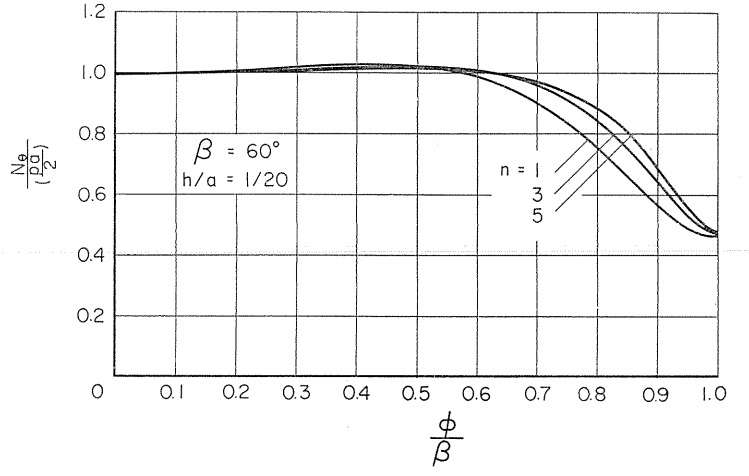

FIG. 2.10. The circumferential component of membrane force.

Finally, the distribution of $M_\phi/(pah/2)$ is shown in Fig. 2.11. The maximum values of $M_\phi/(pah/2)$ occur at the clamped edge, and are 0.190 ($n=1$), 0.128 ($n=3$) and 0.110 ($n=5$), respectively. Thus, the bending stress on the surface of the clamped edge corresponding to these maximum values of $M_\phi/(pah/2)$ in the present shell are 1.211 ($n=1$), 0.533 ($n=3$) and 0.393 ($n=5$) times as large as the membrane stress due to $N_\phi/(pa/2)$ at the edge. It follows, accordingly, that the bending moment in the present shell has a significant effect on the strength of the shell. $M_\theta/(pah/2)$, on the other hand, shows the similar distribution to Fig. 2.11, except that its value at the clamped edge are half of that of $M_\phi/(pah/2)$.

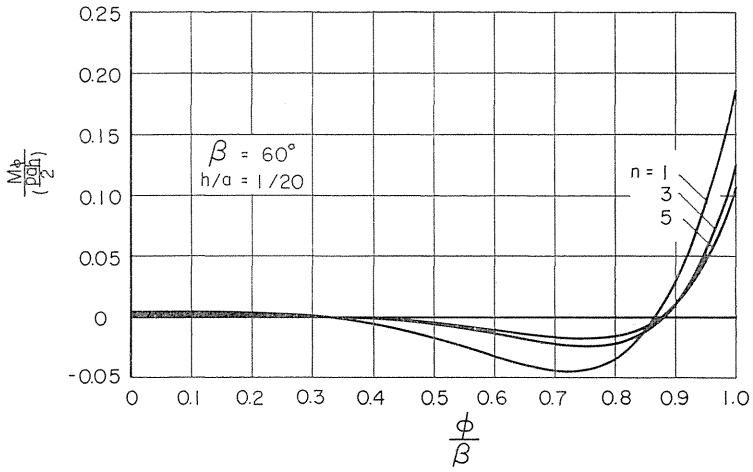

FIG. 2.11. The meridional component of bending moment.

By comparing Fig. 2.9 with Figs. 2.10 and 2.11, it will follow that the components of displacement are affected remarkably by the end condition over the whole shell while the state of stress has the influence of the condition only in the vicinity of the clamped edge and coincides practically with that of complete sphere in the central part of the shell.

The relation (2.4b) may be a constitutive equation of strain-hardening material if the deformation theory of plasticity is assumed. The preceding results, therefore, can also be interpreted as the results for elastic-plastic shells subject to monotonously increasing internal pressure. The present method of numerical analysis, of course, directly applicable also to the physically non-linear problems with more complicated type of constitutive equations than (2.4b). It is, furthermore, applicable to the case of large deflection, too.

5. Conclusion

The extended Newton method combined with the method of finite-difference was shown to be a powerful means to the creep analysis of shells of revolution. Calculations were performed for three kinds of shells on the assumption of the Mises criterion and the power creep law.

In a simply supported pressurised shell of $\alpha=2\pi$ with open end, the largest deflections occur in the region $0.5<2x/l<0.7$ and are larger than the deflection of

thin circular tube in disregard of the end effect by 6 ($n=1$) ~10 ($n=5$) per cent. The larger is the values of n, the wider is the region affected by the end condition. The central part of the shell is almost in the state of hoop stress. In the case of $n=1$, especially, the present results agree with the corresponding analytical one within the accuracy of 0.5 per cent. Moreover, the present results for the maximum deflection and the maximum bending moment in axial direction coincide with the corresponding ones of semi-infinite sandwich shell due to Yu. N. Rabotnov within the accuracy of 0.5 ($n=1$), 7 ($n=3$) and 10 ($n=5$) per cent, respectively.

Similar calculations were also carried out for a clamped circular cylindrical shell. It was observed that the influence of the end condition in the clamped shell prevails over wider region than in the supported one. The maximum values of deflection and the membrane force in the circumferential direction are smaller than in the previous shell by 2 ($n=1$) ~5 ($n=5$) and 2 ($n=1$) ~1 ($n=5$) per cent.

The numerical results for the clamped shell were again compared with the existing solution for sandwich shells due to F. A. Cozzarelli *et al.* In the present shell, the difference in maximum values of the displacement, the bending moment and the membrane force between the uniform and the sandwich shell was less than 3 ($n=1$), 5 ($n=3$) and 10 ($n=5$) per cent although considerable discrepancies between these two kinds of results exist locally near the clamped end where the bending moment and the membrane force coexist in comparable magnitude. The sandwich model, therefore, may give close qualitative and quantitative assesments of the creep deformation of cylindrical shell of the present condition. However, the assumption of the sandwich shell may not always be a good approximation to certain kinds of shells of uniform wall, especially for large value of the creep exponent n.

As the last example, a clamped spherical shell of $\beta=60°$, $h/a=1/20$ was adopted. It was found that the present results for deflection and the bending moment in meridional direction in case of $n=1$ differed from the analytical ones by about 1 per cent of their maximum values. The accuracy of the present analysis, therefore, was a little worse than that for the cylindrical shells. The deflection of the present shell is larger than that of the complete shell by about 40 ($n=1$) ~25 ($n=5$) per cent. The bending stress on the surface of clamped edge corresponding to the maximum values of $M_\phi/(pah/2)$ are 1.211 ($n=1$) ~0.393 ($n=5$) times as large as the membrane stress due to $N_\phi/(pa/2)$ at the edge. Accordingly, the bending moment in the present shell has a significant effect on the strength of the shell, which is, however, significant only in the vicinity of the clamped edge.

Concluding Remarks

Although a number of papers have been published so far concerning the creep deformation of various constructional elements, the works on creep of shells have been relatively scarce and are still a rather new objectives in this field of research. This stems from the fact that the stress resultants in shells cannot be expressed as simple functions of the components of strain or displacement on account of the non-linearity of creep law and analytical approaches are intractable. The past researches on the creep analysis of shells, therefore, were mainly restricted to approximate ones based on certain simplifications.

In the present paper, we developed a numerical approach to the accurate analyses of creep in general shells of revolution by the method of finite-difference, and revealed the certain features of creep of shells employed under the condition of high temperature and high stress. This line of approach seems important from engineering point of view.

In transient creep analysis developed in Part I, the instantaneous elastic strain must be also taken into account at the same time, and hence the effect of creep strain appears only as the inhomogeneous terms in the governing differential equations. In such a kind of problems, similar method as that in elastic problems can be applied if the similar concept as the Duhamel-Neumann's analogy in thermo-elasticity is employed. According to the numerical results for pressurised circular cylindrical shells, it was found that the difference of nearly 100 per cent may occur among the predictions of deflection on account of the difference of creep theories. The Tresca-Tresca theory which predicts larger values of deflection does not necessary give larger values of stresses. It is difficult, therefore, to single out a creep theory among the classical ones which gives the data of safer side in creep design. A certain modification seems necessary to the classical theories of creep in order to estimate the creep accurately. It should be noticed, furthermore, that the difference between the predictions of creep in circular cylindrical shell due to the strain-hardening and the time-hardening hypothesis is sufficiently small if the variation of stress corresponds only to their redistribution under constant pressure.

The numerical results of steady-state creep analyses in Part II were presented in non-dimensional form, and do not involve explicitly the creep constants nor the individual dimensions of shells (except the geometrical parameter of the shells). These results have a general validity to the circular cylindrical shells or the partial spherical shells corresponding to the specified geometrical parameter, and will be useful to infer the behaviour of these shells or as design data to pressure vessels. According to the comparison between the present results for cylindrical shells and the corresponding approximate ones due to sandwich assumption, both kinds of results agree well with each other when the membrane force or bending moment is predominant separately. When membrane force and bending moment coexist in comparable magnitude, however, considerable discrepancies were found between these two kinds of analyses. Though the approximate analyses based on the sandwich assumption is interesting mathematically in the sence that the results are analytical, it is not always practical because it may involve significant errors in certain kinds of problems.

Although the creep theory of Mises type, the power creep law and the small

deflection theory of shell were assumed in the analysis of Part II, the present procedure can be applied also to other kinds of creep theories, more general constitutive equations or to the case of large deformation of shells. The extended Newton method combined with the method of finite-difference employed in the present paper will be a powerful means to the numerical analysis of physically non-linear problems.

Acknowledgement

The present author wishes to express his sincere gratitude to Professor Y. Ohashi of Department of Mechanical Engineering for his invaluable guidance and stimulating discussions concerning this work.

References

1) S. Murakami and S. Iwatsuki, Transient creep deformation of pressurised circular cylindrical shells. Trans. JSME, Vol. **35**, No. 271 (March 1969), 459-469 (in Japanese).
2) S. Murakami and S. Iwatsuki, Transient creep of circular cylindrical shells. Internat. J. Mech. Sci., Vol. **11**, No. 11 (Nov. 1969), 897-912.
3) S. Murakami and S. Iwatsuki, Transient creep analysis of pressurised circular cylindrical shells, Bull. JSME, Vol. **12**, No. 54 (Dec. 1969), 1270-1278.
4) S. Murakami, The application of the finite-difference method to creep deformation in circular cylindrical shells. Rozprawy Inzyniersky, Vol. **18**, No. 4 (1970), 629-674 (in Polish).
5) S. Murakami and S. Iwatsuki, Steady-state creep analysis of circular cylindrical shells. Trans. JSME, Vol. **36**, No. 291 (Nov. 1970), 1761-1771 (in Japanese).
6) S. Murakami and S. Iwatsuki, Steady-state creep of circular cylindrical shells. Bull. JSME, Vol. **14**, No. 73 (July 1971), 615-623.
7) S. Murakami and K. Suzuki, On the creep analysis of pressurised circular cylindrical shells. Internat. J. Non-Linear Mech., Vol. **6**, No. 3 (June 1971), 377-392.
8) S. Murakmi and K. Suzuki, Steady-state creep of clamped circular cylindrical shells subjected to internal pressure. Trans. JSME, Vol. **37** (Nov. 1971), (in Japanese).
9) S. Murakami and K. Suzuki, Application of the extended Newton method to the creep analysis of shells of revolution. Ingenieur-Archiv (in press).
10) R. K. Penny, The creep of spherical shells containing discontinuties. Internat. J. Mech. Sci., Vol. **9**, No. 6 (June 1967), 373-388.
11) R. K. Penny, The creep of pressurised cylindrical shells. J. Roy. Aero. Soc., Vol. **73** (June 1969), 514-519.
12) R. K. Penny, The creep of shells. Proc. 2nd IUTAM Symp. on Creep in Structures, Gothenburg (1970) (in press).
13) A. E. Johnson and B. Khan, Creep under changing complex-stress systems in copper at 250°C. Internat. J. Mech. Sci., Vol. 7, No. 12 (Dec. 1965), 791-810.
14) I. Finnie and W. R. Heller, Creep of Engineering Materials, McGraw-Hill, New York (1959).
15) F. K. G. Odqvist and J. Hult, Kriechfestigkeit metallischer Werkstoffe, Springer, Berlin (1962).
16) Yu. N. Rabotnov, Creep Problems in Structural Members, North-Holland, Amsterdam (1969).
17) F. Garofalo, Fundamentals of Creep and Creep Rupture in Metals, MacMillan, New York (1965).
18) A. M. Wahl, Effects of the transient period in evaluating rotating disk test under creep conditons. Trans. ASME, Ser. D, J. Basic Engng, Vol. **85**, No. 1 (March 1963), 66-70.
19) A. M. Wahl, Application of the modified Bailey equations for creep under biaxial stress. Proc. 4th U. S. Nat. Congr. Appl. Mech., ASME, New York (1962), 1167-1173.

20) A. E. Gemma, G. H. Rowe and R. J. Spahl, Elastic and creep characteristics of a class of shell closures with constant stress ratio. Trans. ASME, Ser. D. J. Basic Engng, Vol. **81** (1959), 599.
21) S. Timoshenko and S. Woinowsky-Krieger, Theory of Plates and Shells (2nd ed.), MacGraw-Hill, New York (1959).
22) M. Soare, Application of Finite-Difference Equations to Shell Analysis, Pergamon, Oxford (1967).
23) H. Kraus, Thin Elastic Shells, John Wiley, New York (1967).
24) G. E. Forsythe and W. R. Wasow, Finite-Difference Methods for Partial Differential Equations, John Wiley, New York (1966).
25) A. Ralston and H. S. Wilf, Mathematical Methods for Digital Computers, John Wiley, New York (1960).
26) W. Olszak and A. Sawczuk, Inelatic Behaviour in Shells, P. Noordhoff, Groningen (1967).
27) E. T. Onat and H. Yüksel, On the steady creep of shells. Proc. 3rd U. S. Nat. Congr. Appl. Mech., ASME, New York (1958), 625-630.
28) M. P. Bieniek and A. M. Freudenthal, Creep deformation and stresses in pressurized long cylindrical shells. J. Aerospace Sci., Vol. **27**, No. 10 (Oct. 1960), 763-778.
29) V. I. Rozenblyum, Approximate equations of creep of thin shells. Prikl. Math. Mekh., Vol. **27**, No. 1 (1963), 154-160,
30) C. R. Calladine and D. C. Drucker, Nesting surfaces of constant rate of energy dissipation in creep. Quart. Appl. Math., Vol. **20** (1962), 79-84.
31) C. R. Calladine, Edge-load response of a thin cylindrical shell in creep. Non-Classical shell Problems, North-Holland, Amsterdam (1964), 384-408.
32) C. R. Calladine, Creep in torispherical pressure vessel heads. Proc. 2nd IUTAM Symp. On Creep in Structures, Gothenburg (1970), (in press).
33) I. G. Teregulov, On variational methods of solution of steady creep problems for plates and shells at large deflections. Prikl. Math. Mekh., Vol. **26** (1962), 492-496.
34) I. G. Teregulov, Creep in edge zones of thin shells. Izv. AN SSSR, Mekh. Mashinostr., No. 6 (1963), 169-173.
35) Yu, N. Rabotnov, Axisymmetrical creep problems of circular cylindrical shells. Prikl. Math. Mekh., Vol. 28, No. 6 (1964), 1040-1047.
36) Yu. N. Rabotnov, Creep of shells. Proc. 11th Internat. Congr. Appl. Mech., Springer, Berlin (1966), 415-419.
37) Yu. M. Volchkov, Axisymmetric problems of creep in circular cylindrical shells. Izv. AN SSSR, Mekh. Mashinostr., No. 5 (1965), 118-121.
38) A. E. Gemma, The creep deformation of symmetrically loaded circular cylindrical shells. J. Aerospace Sci., Vol. **27**, No. 12 (Dec. 1960), 953-954.
39) A. E. Gemma, The steady creep of long pressurized cylinders. J. Aerospace Sci., Vol. **29**, No. 3 (March 1962), 352-353.
40) F. A. Cozzarelli, S. A. Patel and B. Venkatraman, Creep analysis of circular cylindrical shells, AIAA J., Vol. **3**, No. 7 (July 1965), 1298-1301.
41) T. P. Byrne and A. C. Mackenzie, Secondary creep of a cylindrical thin shell subject to axisymmetric loading. J. Mech. Engng. Sci., Vol. 8 (1966), 216.
42) R. E. Bellman and R. E. Kalaba, Quasi-Linearization and Non-Linear Boundary Value Problems, Elsevier, New York (1965).
43) J. R. Radhill and G. A. McCue, Quasi-Linearization and Non-Linear Problems in Fluid and Orbital Mechanics, Elsevier, New York (1970).
44) G. A. Thurston, Newton's method applied to problems in non-linear mechanics. Trans. ASME, Ser. E, J. Appl. Mech., Vol. **32**, No. 2 (June 1965), 383-388.
45) G. A. Thurston, Continuation of Newton's method through bifurcation points. Trans. ASME, Ser. E, J. Appl. Mech., Vol. **36**, No. 3 (Sept. 1969), 425-430.
46) N. J. Hoff, Approximate analysis of structures in the presence of moderately large creep deformations. Quart. Appl. Math., Vol. **12**, No. 1 (Apr. 1954), 49-55.
47) T. H. Lin, Theory of Inelastic Strucures, John Wiley, New York (1968).